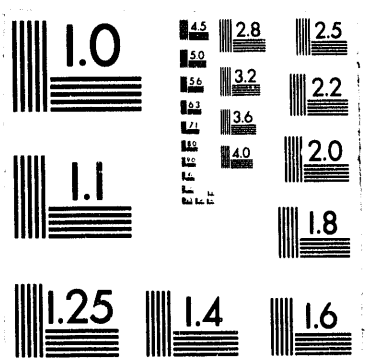
1.0
1.1
1.25
1.4
1.6
1.8
2.0
2.2
2.5
2.8
3.2
3.6
4.0
4.5
5.0
5.6
6.3
7.1

1 of 1

DOE/MC/26288-3688 MTCI 10050-13

# TECHNICAL PROGRESS REPORT

## October 1993 - December 1993

For:

**U.S. Department of Energy**
**~~Pittsburgh~~ Morgantown Energy Technology Center**

Under:

**DOE Contract No. ~~DE-AC22-90PC90155~~ DE-AC21-89MC26288**

**~~Development and Testing of Commercial-Scale, Coal-Fired Combustion Systems: Phase III~~**
**Sonic Enhanced Ash Agglomeration and Sulfur Capture**

By:

MANUFACTURING AND TECHNOLOGY CONVERSION INTERNATIONAL, INC.
P.O. Box 21, Columbia, Maryland 21045-0021

# PREFACE

This 18th Quarterly Technical Progress Report presents the results of work accomplished during the period September 27, 1993 through January 2, 1994 under Contract No. DE-AC21-88MC26288 entitled "Sonic Enhanced Ash Agglomeration and Sulfur Capture." The fundamental studies conducted by West Virginia University and Penn State University are provided in Subsections 2.2 and 2.3.

During this period, several tests were run for various configurations of the Bimodal System with one being a nine-hour steady-state test on coal. The results of all of the tests indicated that the general performance of the unit in terms of acoustic and combustion efficiency was much like the previous tests, 99.5% combustion efficiency at 183 dB. In some instances, sulfur capture was improved. $NO_x$ emissions exceeded the 150 ppm @ 15% $O_2$ goal except for one test.

# TABLE OF CONTENTS

# LIST OF FIGURES

## LIST OF FIGURES
(CONT'D)



## LIST OF TABLES

# SECTION 1.0

# INTRODUCTION

## 1.1 PROJECT DESCRIPTION AND WORK STATUS

A major concern with the utilization of coal in directly fired gas turbines is the control of particulate emissions and reduction of sulfur dioxide, and alkali vapor from combustion of coal, upstream of the gas turbine. Much research and development has been sponsored on methods for particulate emissions control and the direct injection of calcium-based sorbents to reduce $SO_2$ emission levels. The results of this research and development indicate that both acoustic agglomeration of particulates and direct injection of sorbents have the potential to become a significant emissions control strategy.

The Sonic Enhanced Ash Agglomeration and Sulfur Capture program focuses upon the application of an MTCI proprietary invention (Patent No. 5,197,399) for simultaneously enhancing sulfur capture and particulate agglomeration of the combustor effluent. This application can be adapted as either a "hot flue gas cleanup" subsystem for the current concepts for combustor islands or as an alternative primary pulse combustor island in which slagging, sulfur capture, particulate agglomeration and control, and alkali gettering as well as $NO_x$ control processes become an integral part of the pulse combustion process.

The goal of the program is to support the DOE mission in developing coal-fired combustion gas turbines. In particular, the MTCI proprietary process for bimodal ash agglomeration and simultaneous sulfur capture will be evaluated and developed. The technology embodiment of the invention provides for the use of standard grind, moderately beneficiated coal and WEM for firing the gas turbine with efficient sulfur capture and particulate emission control upstream of the turbine. The process also accommodates injection of alkali gettering material if necessary. This is aimed at utilization of relatively inexpensive coal fuels, thus realizing the primary benefit being sought by direct firing of coal in such gas turbine systems. The proposed technology provides for practical, reliable,

and capital (and O&M) cost-effective means of protection for the gas turbine from impurities in the coal combustor effluent.

## 1.2 PROGRAM OBJECTIVES

The major objective of the Phase I test program is to confirm the feasibility of the MTCI bimodal particle size approach to enhance particulate control by acoustic ash agglomeration. An ancillary objective of the Phase I effort is to demonstrate and confirm the feasibility of an acoustic field to enhance sulfur capture by increasing sorbent reactivity. Phase I tests are designed to cover the frequency range between 50 and 1400 Hz, establish monomodal baseline performance as a benchmark from which to measure the degree of enhancement expected from the bimodal approach, and, finally, to confirm the effectiveness of low-frequency fields over high-frequency fields for realistic particulate streams.

The program will demonstrate the effectiveness of a unique approach which uses a bimodal distribution composed of large sorbent particles and fine fly ash particles to enhance ash agglomeration and sulfur capture at conditions found in direct coal-fired turbines. Under the impact of high-intensity sound waves, sorbent reactivity and utilization, it is theorized, will increase while agglomerates of fly ash and sorbents are formed which are readily collected in commercial cyclones. The work will extend the concept from the demonstration of feasibility (Phase I), through proof-of-concept (Phase II) to the construction (Phase III) of a coal-fired pulsed combustor with in-furnace sorbent injection. For Phase I, Pennsylvania State University will conduct studies for enhanced sulfur capture in The Combustion Laboratory and agglomeration tests in the High Intensity Acoustic Laboratory.

## 1.3 SUMMARY STATUS FOR THE PERIOD

During this period, several tests were run for various configurations of the Bimodal System with one being a nine-hour steady-state test on coal. The results of all of the tests indicated that the general performance of the unit in terms of acoustic and combustion efficiency was much like the previous tests, 99.5% combustion efficiency at 183 dB. In some instances, sulfur capture was improved. $NO_x$ emissions exceeded the 150 ppm @ 15% $O_2$ goal except for one test.

# SECTION 2.0

# TECHNICAL DISCUSSION OF THE WORK ACCOMPLISHED DURING THE REPORTING PERIOD

## 2.1 TASK 1: SHAKEDOWN TESTING

SCREENING TESTS

During this reporting period, the MTCI PAFBC system was used to calcine and classify Dolofil 4060 limestone for bimodal tests. The limestone was fed into the pulse combustion chamber. Natural gas was fired in the combustion chamber (0.9 MMBtu/hr), bed windbox (1.1 MMBtu/hr), and freeboard (0.25 MMBtu/hr).

The temperature in the combustion chamber without limestone feed was about 2050°F. With limestone feed, the temperature in the combustion chamber was about 1850°F, in the bed area between 1650 and 1750°F and in the freeboard, approximately 1500°F.

A total of 640 pounds of classified and calcined sorbent was prepared for the bimodal tests. A sample was sent to SSM Laboratories for particle size-BAHCO analysis. The results of the analysis are shown in Figures 1(a) and 1(b). On a weight basis, about 70 percent of the particles were below 10 microns in size. Chemical analysis of the calcined sample by Penn State University indicated the extent of calcination to be about 70 percent.

Several attempts were made to run steady-state tests on the bimodal system but without success. The combustor pulsed normally for awhile (1-4 hrs) but then suddenly failed. After a few restarts and failures, the entire system was examined and inspected. The inspection showed that the Macawber coal-feeding system did not work properly; diagnostic tests were run on the feeder and the problem was traced to the leakage of the seal between the lock and injector vessels. The leakage interrupted the coal feed and caused flame out. The sealing system was debugged and the pneumatic sealing valve was found to be defective. The valve was taken apart and the defect was identified and corrected.

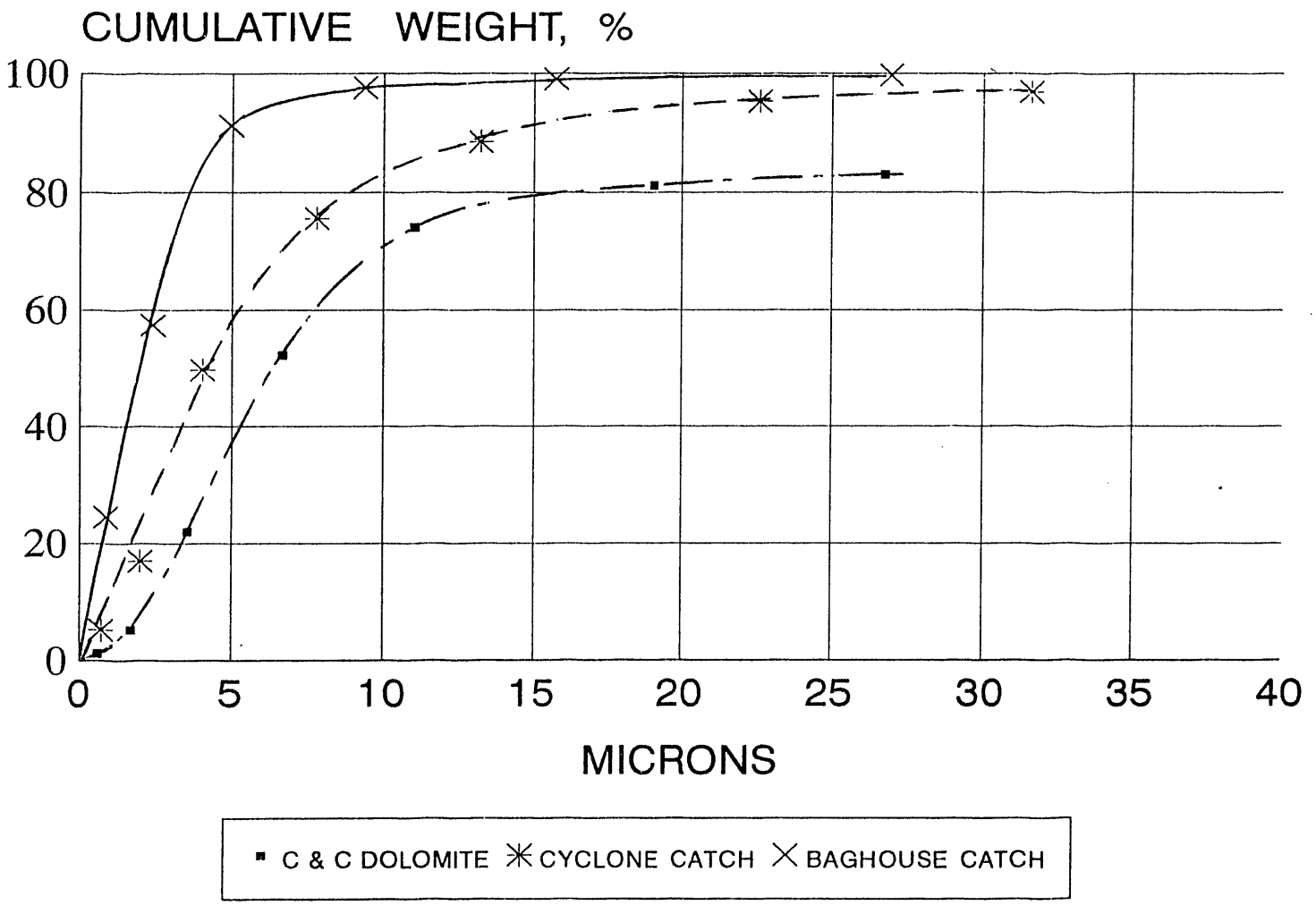


**FIGURE 1-A: BAHCO SIZE DISTRIBUTION**

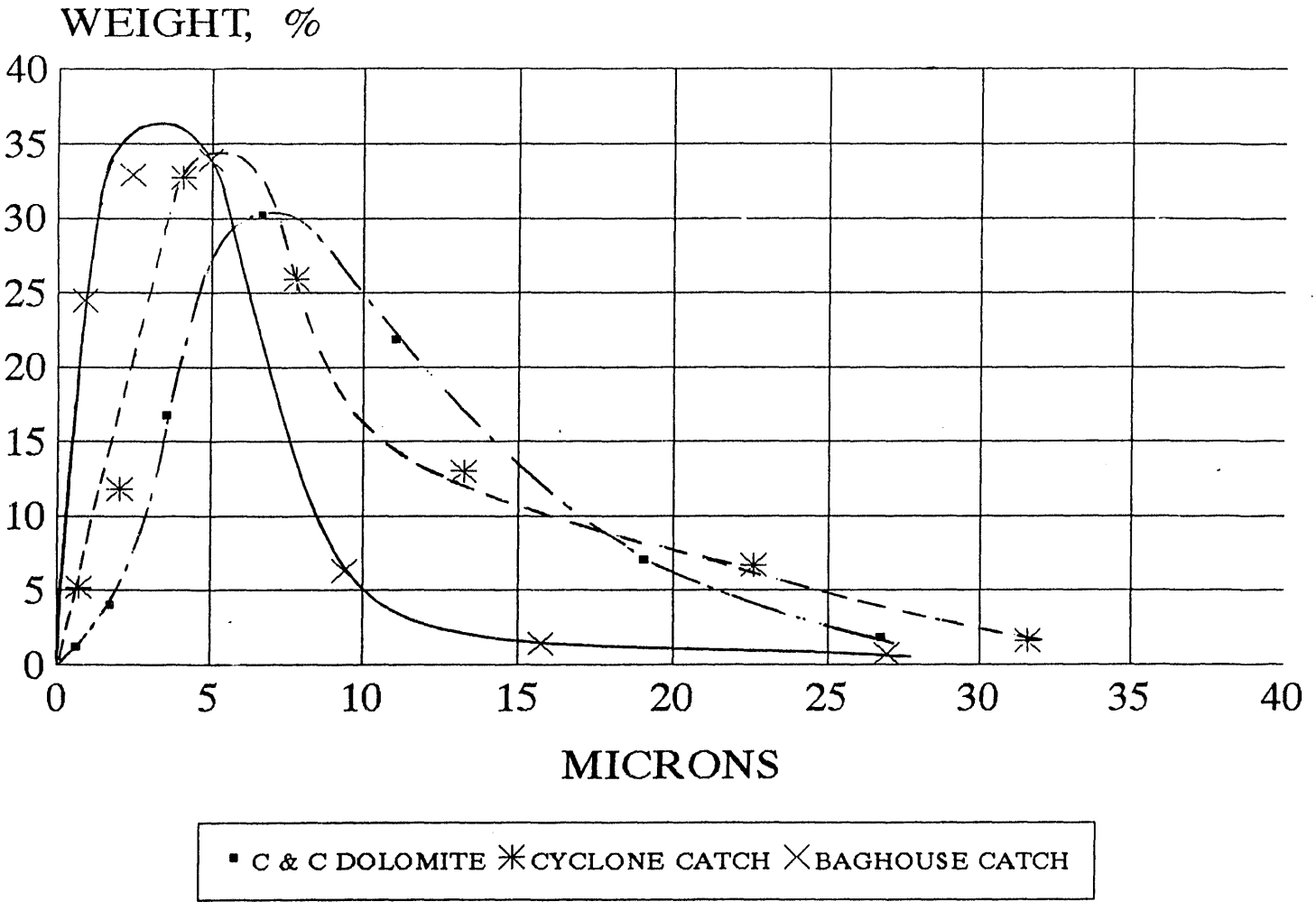


**FIGURE 1-B: BAHCO SIZE DISTRIBUTION**

The leakage interrupted the coal feed and caused flame out. Another problem was found in the pilot gas rotameter. The needle valve of the rotameter was malfunctioning and did not meter the correct flow rate. The rotameter was replaced. At the same time the pilot burner spark plug and flame rod and the combustion chamber ultraviolet flame sensor were replaced with new ones. Tests on the bimodal unit were then resumed.

A test with only coal feed was performed on November 3, 1993. The steady-state condition was sustained for 9 hours. The typical set of data are shown in **Table 1** (Test No. 11032). The system pressure was 3 atm. The temperature in the combustion chamber was about 2250°F and at the bottom of the agglomeration chamber it was 2000°F. The acoustic performance was good (183 dB) and the combustion efficiency was 99.5 percent. The cyclone and baghouse catch samples were sent for BAHCO size analysis. The results of the analysis are shown in Figures 1(a) and 1(b). Approximately 25 percent by weight of particles collected in the baghouse exceeded 3 microns in size. Isokinetic particulate samples showed that solids loading after the cyclone was on average 141 ppmw.

A power spectra taken during pulse combustion operation indicated a strong first harmonic in addition to the fundamental frequency (~ 88 Hz) and it was decided to examine whether the reflection cone at the bottom of the agglomeration chamber was a contributing factor. Therefore, the flange at the bottom of the agglomeration chamber was disassembled, the reflection cone was cut off, the outlet at the bottom of the chamber was closed, and the flange reassembled. A test was performed in this configuration first with coal feed only and then with coal and Dolomite. General performance of the bimodal unit in the test (denoted as test set 1) in terms of acoustic and combustion efficiency was as before. Sulfur capture with Dolomite was higher than 90 percent (see Figure 2, test set 1). However, the solids loading after the cyclone in the test was higher than in previous tests (see Table 1, Test Nos. 12061 and 12062). Due to the increased open area at the bottom of the agglomeration chamber, the flow velocity decreased as also the entrained solids rate. This decreased solids concentration in the outer annulus of the agglomeration chamber reduced the agglomeration effectiveness and increased the cyclone exit solids loading. The sulfur capture however

## TABLE 1. TEST RESULTS SUMMARY OF BIMODAL PROJECT FIRING WITH COAL

| Test No. | | | 11032 | 12061 | 12062 | 12063 | 12081 | 12082 | 12083 | 12084 | 12085 | 12161 | 12162 |
|---|---|---|---|---|---|---|---|---|---|---|---|---|---|
| Test set No. | | | | 1 | 1 | 1 | 2 | 2 | 2 | 2 | 2 | 3 | 3 |
| Number of cyclones | | | 1 | 1 | 1 | 1 | 1 | 1 | 1 | 1 | 1 | 2 | 2 |
| Firing rate | Total, MMBtu/Hr | | 2.42 | 2.16 | 2.16 | 2.16 | 2.27 | 2.27 | 2.27 | 2.27 | 2.27 | 2.24 | 2.25 |
| | Coal, % | | 70.1 | 78.5 | 78.4 | 78.4 | 78.2 | 78.2 | 78.2 | 78.2 | 78.2 | 77.9 | 77.7 |
| | Natural gas, % | | 29.9 | 21.5 | 21.6 | 21.6 | 21.8 | 21.8 | 21.8 | 21.8 | 21.8 | 22.1 | 22.3 |
| Sorbent | Feeding rate, lb/hr | | 0.0 | 0.0 | 22.5 | 30.0 | 0.0 | 22.5 | 30.0 | 43.2 | 52.5 | 0.0 | 70.0 |
| | Feeding location | | A.C. | A.C. | A.C. | A.C. | A.C. | A.C. | A.C. | A.C. | A.C. | A.C. | A.C. |
| Temperature, F | Air plenum | | 158 | 146 | 146 | 147 | 143 | 145 | 144 | 144 | 144 | 146 | 145 |
| | Combustion chamber | | 2254 | 2308 | 2301 | 2315 | 2340 | 2225 | 2321 | 2347 | 2247 | 2470 | 2439 |
| | Bottcm of agglomeration chamber | | 2005 | 1907 | 1911 | 1920 | 2021 | 2116 | 2171 | 2208 | 2225 | 2055 | 1890 |
| | Exit of agglomeration chamber | | 1424 | 1350 | 1352 | 1359 | 1421 | 1455 | 1523 | 1509 | 1504 | 1459 | 1510 |
| | Exit of cyclone | | 1077 | 961 | 981 | 972 | 971 | 1001 | 1035 | 1037 | 1035 | 1058 | 1068 |
| | Exit of heat exchanger | | 500 | 455 | 472 | 488 | 420 | 453 | 396 | 426 | 448 | 447 | 516 |
| | Steam | | 275 | 275 | 276 | 276 | 276 | 276 | 276 | 275 | 275 | 278 | 277 |
| Pressure, psia | Air plenum | | 44.7 | 45.1 | 45.4 | 45.6 | 45.3 | 46.0 | 45.7 | 44.9 | 45.4 | 45.7 | 45.7 |
| | Combustion chamber | | 44.8 | 44.8 | 45.3 | 45.3 | 44.9 | 44.9 | 45.0 | 44.6 | 45.1 | 45.2 | 45.4 |
| | Cyclone inlet | | 44.7 | 44.6 | 45.0 | 45.1 | 44.7 | 44.7 | 44.7 | 44.4 | 44.7 | 44.8 | 45.2 |
| | Cyclone outlet | | 44.5 | 44.4 | 44.6 | 44.8 | 44.4 | 44.4 | 44.6 | 44.1 | 44.6 | 44.6 | 44.9 |
| | Steam drum | | 44.0 | 44.1 | 44.2 | 44.2 | 44.1 | 44.1 | 44.0 | 44.0 | 43.9 | 44.1 | 44.2 |
| Excess air, % | | | 9.9 | 8.2 | 13.5 | 15.4 | 3.4 | 7.1 | 7.7 | 8.2 | 6.6 | 14.2 | 15.4 |
| Emission data of stack (corrected to 3 % O2) | O2. % | | 1.9 | 1.6 | 2.5 | 2.8 | 0.7 | 1.4 | 1.5 | 1.6 | 1.3 | 2.6 | 2.8 |
| | CO2, % | | 14.9 | 14.6 | 13.8 | 13.6 | 15.4 | 14.8 | 14.9 | 14.6 | 14.9 | 13.6 | 13.6 |
| | CO, ppm | | 6 | 15 | 11 | 7 | 53 | 7 | 10 | 11 | 3 | 8 | 4 |
| | SOx, ppm | | 711 | 648 | 54 | 12 | 708 | 257 | 114 | 102 | 30 | 823 | 79 |
| | NOx, ppm | | 332 | 429 | 519 | 529 | 417 | 549 | 582 | 570 | 601 | 506 | 597 |
| | HC, ppm | | 2 | 2 | 3 | 1 | 2 | 1 | 2 | 3 | 5 | 1 | 1 |
| Acoustic data | Combustion chamber | SPL, db | 183 | 181 | 181 | 181 | 181 | 180 | 181 | 181 | 179 | 181 | 180 |
| | | Frequenc | 88 | 84 | 84 | 84 | 86 | 84 | 84 | 84 | 80 | 84 | 84 |
| Combustion efficicncy, % | | | >99 | >99 | >99 | >99 | >99 | >99 | >99 | >99 | >99 | >99 | >99 |
| Particulate emissions, PPMW | | | 141 | 163 | 309 | 275 | 134 | 289 | 272 | 259 | 241 | 32 | 72 |

improved due to greater particle accumulation at the bottom of the agglomeration chamber.

It was decided after the test to reinstall the reflection cone at the bottom of the agglomeration chamber and continue the tests. A test was performed on December 8, 1993 (denoted as test set 2). The test data are shown in Table 1 (Test Nos. 12081 and 12082) and Figures 2, 3, and 4 (test set 2). The data show that combustion chamber temperature was about 2350°F and the temperature at the bottom of the agglomeration chamber was 2021°F with coal feed only and 2200°F with coal and limestone feed. Combustion efficiency was 99.5 percent. Sulfur capture was less than that in the test without the reflection cone (65 to 95%). Higher sulfur capture in that test can be explained by lower velocity of flue gases at the bottom of the agglomeration chamber and longer residence time of the limestone particles. But in the reflection cone test, the agglomeration occurred better and solids loading was lower (134 ppmw with coal only and 259 ppmw with coal and Dolomite feed).

All these tests showed that the existing system did not achieve low enough (< 100 ppmw) solids loading at the exit of the system. Due to concerns about possible agglomerate breakup, a modest velocity (55 ft/s) was used in sizing the inlet and designing the existing cyclone. A second high efficiency cyclone was considered necessary to reduce both solids loading and the carryover of larger particles (> 3 microns). Therefore, a new high efficiency cyclone was designed, fabricated and installed upstream of the pressure letdown valve of the system.

During the test of the bimodal unit with the second cyclone, the limestone feeder motor burned out. The limestone feed system was therefore disassembled and a new motor was installed. The motor and gear box were covered with sheet metal enclosure and the sorbent transport air was supplied through this enclosure into the pressure vessel to keep dust away from the motor during use. The limestone feed system was reassembled back and the limestone feeder recalibrated. A test (denoted as test set 3) was performed on the new system. The test data are shown in Table 1 (last two columns) and in Figures 2, 3 and 4 (test set 3).

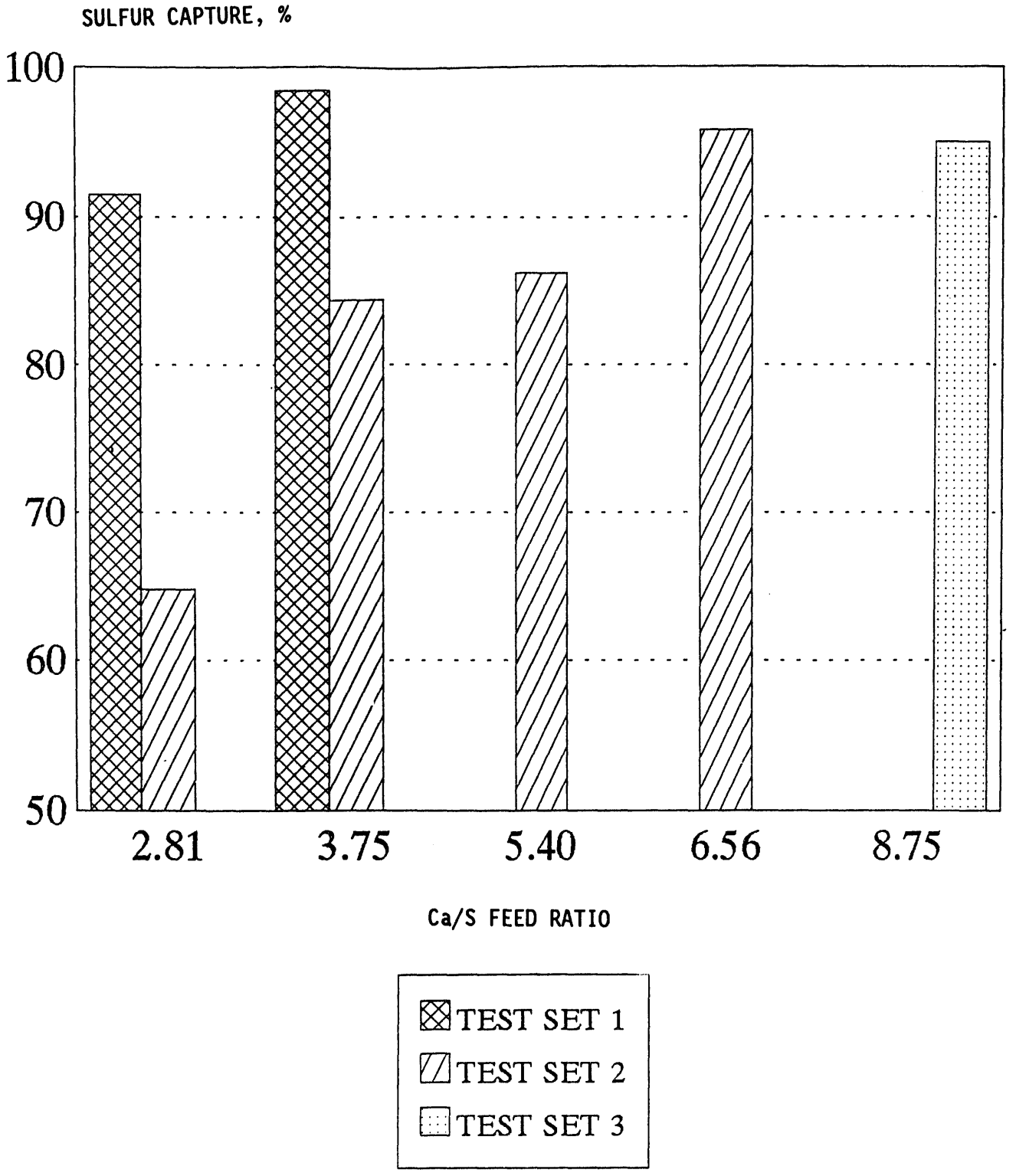


**FIGURE 2: SULFUR CAPTURE WITH DOLOMITE**

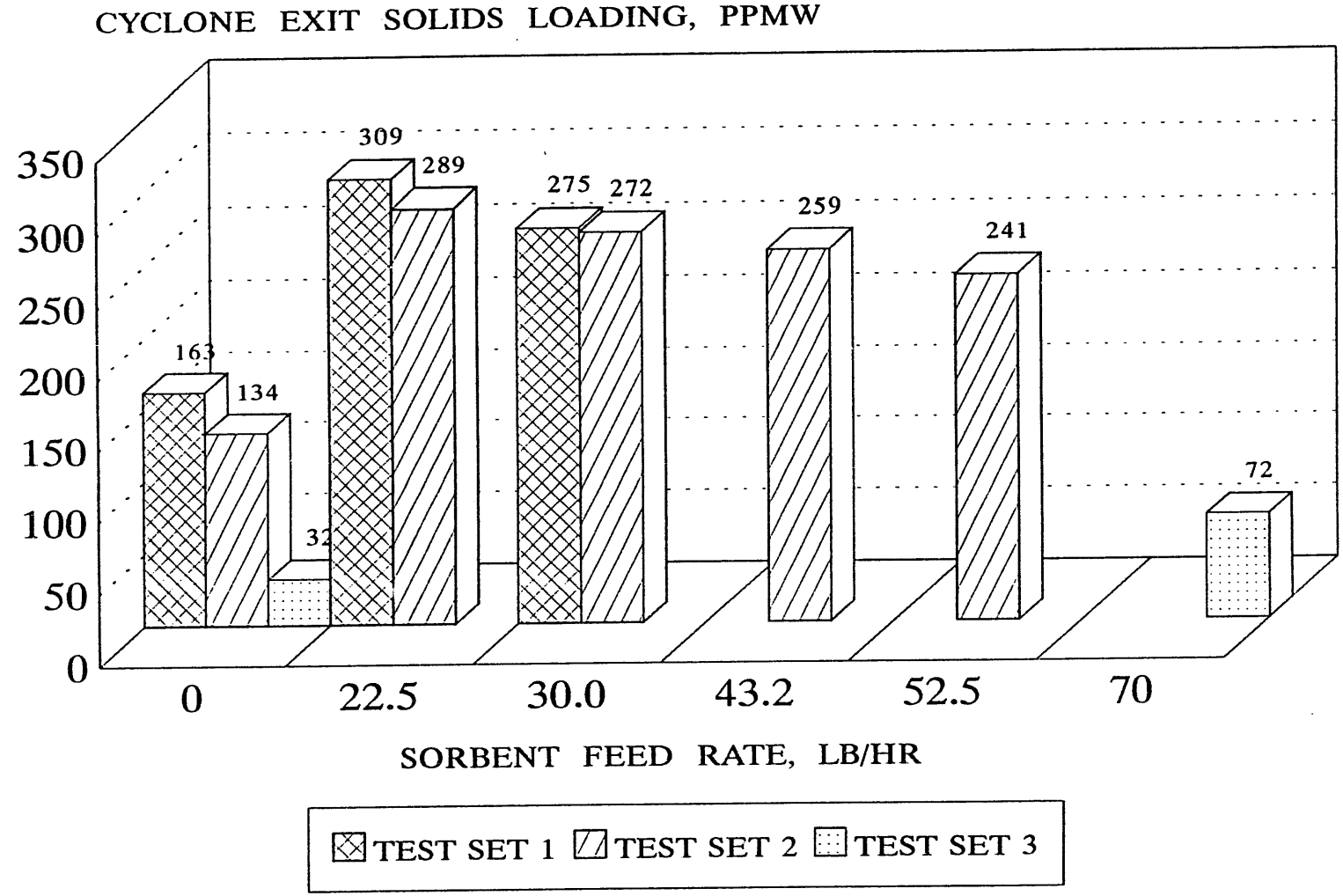


**FIGURE 3: CYCLONE EXIT SOLIDS LOADING WITH COAL AND SORBENT FEED**

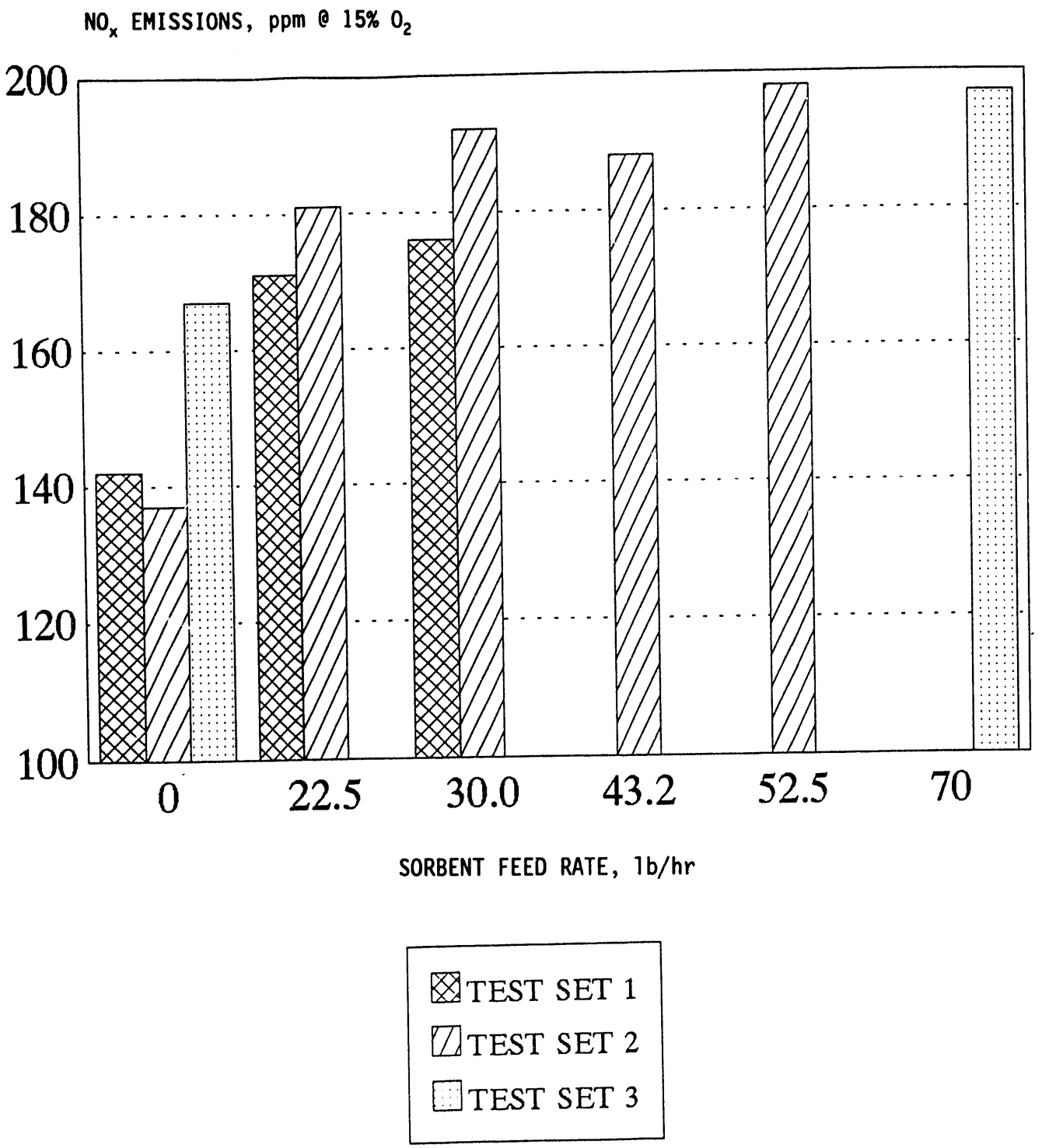


**FIGURE 4: $NO_x$ EMISSIONS WITH COAL AND SORBENT FEED**

The temperature in the combustion chamber was about 2450°F. Acoustic performance and combustion efficiency were the same as in previous series of tests. Sulfur capture was 95 percent but with high Ca/S ratio (8.75:1). Solids loading after the second cyclone was very low (32 ppmw with coal feed only and 72 ppmw with coal and Dolomite feed). The higher loading with sorbent feed is attributed to enhanced fines loading (21% by weight of sorbent below 3 microns), possible fragmentation of the sorbent in the agglomeration chamber, and less effective sorbent-sorbent agglomeration. $NO_x$ emissions from all the tests are shown in Figure 4. $NO_x$ emissions exceed the goal of 125 ppm at 15% $O_2$ and substoichiometric operation of the pulse combustor is indicated to achieve the target goal.

Baghouse catch samples typically exhibited the effect of caking and, therefore, in test set 3 efforts were made to collect a representative, dry, uncaked second cyclone exit sample for size analysis. A filter bag was inserted in the bypass line and the baghouse flow was partially diverted to this line. Collection during a 70-minute test interval failed to catch particulates due to high flow velocity and lack of a dust cake layer. Therefore, a new very high efficiency cyclone train (3 cyclones in parallel) in conjunction with a downstream isokinetic sampling line is being designed to collect the cyclone exit solids and perform size analysis.

To ensure that solids loading results of the test are accurate and to obtain samples analysis which will give right size distribution at the end of the bimodal system, a new isokinetic configuration was designed to install after the pressure letdown valve. Three tiny, very high efficiency cyclones will collect samples from the new isokinetic system.

## 2.2 AEROVALVE TEST (WEST VIRGINIA UNIVERSITY)

### 2.2.1 AEROVALVE DESIGN

INCOMPRESSIBLE VISCOUS FLOW IN A VORTEX-TYPE AEROVALVE

The viscous vortex analysis presented here supersedes the previous inviscid models. New nomenclature is needed for description of the flow in the valve since one-dimensional flow no longer exists. The absolute velocity and its radial and tangential components $u_r$ and $u_\theta$ are also needed. The subscript (t) has been used to indicate the total conditions of the flow. The usual (f) and (r) for forward and reverse directions also create problems with (r) already being used for radial components. Stations have been indicated by the subscripts (i), (v), (th), (o), and the forward and reverse directions by (F) and (R). The lone exception is the definition of the area ratio $A_R$, which is the total forward flow exit area $A_o$ at $r_o$ divided by the total throat area $A_{th} = Ns^2$, or $A_o = A_R Ns^2$. Here N is the number of vane passages, each with throat width $s^2$ because the throat is square with width s. The reverse flow exit area is the cylindrical area described by $A_i = 2\pi r_i s$, designed equal to $4A_e$.

CONVENTIONAL QUASI-ONE-DIMENSIONAL FLOW

In a converging-diverging-type aerovalve with reverse flow separating at the throat,

$$\Delta p_F = \frac{1}{2}\rho V_{F_o}^2, \quad or \quad V_{F_o} = \sqrt{\frac{2\Delta p_F}{\rho}} \tag{1.1}$$

and

$$\dot{m}_F = \rho A_{th} A_R V_{F_o} \tag{1.2}$$

where $A_R$ is the venturi exit to throat area ratio. This gives

$$\dot{m}_F = \rho A_{th} A_R \sqrt{\frac{2\Delta p_F}{\rho}} \tag{1.3}$$

For reverse flow separating at the throat with no further pressure recovery

$$\Delta p_R = \frac{1}{2}\rho V_{th}^2, \quad or \quad V_{th} = \sqrt{\frac{2\Delta p_R}{\rho}} \tag{1.4}$$

and

$$\dot{m}_R = \rho A_{th} \sqrt{\frac{2\Delta p_R}{\rho}} \tag{1.5}$$

and the diodicity was defined as the ratio of forward to reverse mass flow rates at the same $\Delta p$:

$$Diodicity \quad D = \frac{\dot{m}_F|_{at\ same\ \Delta p}}{\dot{m}_R} = A_R \tag{1.6}$$

## VISCOUS VORTEX-TYPE AEROVALVE MODEL

The modeling of the vortex strength generated by reverse flow in the aerovalve controls the magnitude of the effect of the vortex ($K_v$) on the magnitude of the diodicity $D_v = A_R K_v (T_R)^{1/2}$. The effect of having one or more separated flow jets entering the vortex chamber at a velocity $V_{thR}$ at area $A_{th}$ and radius $r_{th}$ and angle $\delta$ is to provide an in-flow rate of angular momentum given by $r_{th}\dot{m}_R V_{thR}\cos\delta$. Because the free jet trajectory is unstable, the tangential flow inside the vortex with unknown velocity component $U_{\theta_v}$ will deflect the

separated jet to the wall, thus forcing the jet to make a Coanda-type turning departure out of the vane throat. Once inside the vortex chamber of radius $r_v$, its singular identity is lost as it becomes part of the uniform vortex. Inside the vortex chamber the separated flow jets produce a vortex angular momentum flow rate given by $r_v \dot{m}_R U_{\theta v}$. The wall viscous losses dissipate a portion of the angular momentum in-flow rate. These viscous losses are modeled by the product of the vortex chamber radius ($r_v$) multiplied by the wall area $A_w = [2\pi r_v s + 2\pi(r_v^2 - r_i^2)]$ times the wall shear stress $\tau = C_f \frac{1}{2} \rho U_\theta^2$. The magnitude of the friction coefficient $C_f$ depends on the local Reynolds number and turbulence level. The resulting momentum flow rate balance equation is

$$r_{th} \dot{m}_R (V_{th_R} \cos\delta) - r_v \dot{m}_R U_{\theta v} + r_v A_w C_f \left( \frac{1}{2} \rho U_{\theta v}^2 \right) \tag{1.7}$$

where

$$\dot{m}_R = \rho A_{th} V_{th_R} \tag{1.8}$$

The velocity friction ratio $V_{fr}$ is the vortex maximum tangential velocity $U_{\theta v}$ divided by the tangential component of the jet velocity at the throat, $V_{thR}\cos\delta$. The ratio $A_{wth}$ is equal to $\frac{1}{2} C_f (A_w / A_{th})$, and writing this in the form of a quadratic equation:

$$\frac{r_{th}}{r_v} = \frac{U_{\theta v}}{V_{th_R} \cos\delta} + \frac{A_w}{A_{th}} \frac{C_f}{2} \cos\delta \left( \frac{U_{\theta v}}{V_{th_R} \cos\delta} \right)^2 \tag{1.9}$$

$$V_{fr} = \frac{U_{\theta_v}}{V_{th_R}\cos\delta} = \frac{\sqrt{1 + \frac{4A_{w_{th}} r_{th}\cos\delta}{r_v}} - 1}{2A_{w_{th}}\cos\delta} \tag{1.10}$$

$C_f$ is to be determined experimentally, for example assume: $C_f = 0.1$, $\cos\delta = 0.5$, $A_w$=10 sq." and for N = 2 and s = .5", $A_{th}$=½ sq." and $A_{wth} = 1$. For $r_{th} / r_v = 1.1$ this gives $V_{fr} = 0.79$. Without friction due to conservation of angular momentum ($C_f = 0$), $V_{fr} = r_{th} / r_v$, which must be > 1.0.

The magnitude of $C_f$ could be taken from duct friction factors at a Reynolds number equal that of the reverse flow in the throat. Experimental data are more likely needed to get a handle on the magnitude of $C_f$. The effect of friction on the loss of diodicity from the area ratio $A_R$ can be accounted for with an empirical loss coefficient $C_{th}$. There is then no need to add additional loss factors. The reverse flow pressure drop inside the vortex chamber can then be calculated assuming an inviscid irrotational vortex with tangential flow pressure drop

$$\Delta p_\theta = \frac{1}{2}\rho(U_{\theta_i}^2 - U_{\theta_v}^2) = \frac{1}{2} V_{th_R}^2 V_{fr}^2 \left(\left(\frac{r_v}{r_i}\right)^2 - 1\right) \tag{1.11}$$

The radial two-dimensional sink-type pressure drop is

$$\Delta p_r = \frac{1}{2}\rho\left(U_{r_i}^2 - U_{r_v}^2\right) = \frac{1}{2}\rho U_{r_i}^2\left(1 - \left(\frac{r_i}{r_v}\right)^2\right) - \frac{1}{2}\rho V_{th_R}^2\left(\frac{1}{A_R}\right)^2\left(1 - \left(\frac{r_i}{r_v}\right)^2\right) \tag{1.12}$$

and the vane pressure drop, due to throat separation, using the empirical loss coefficient $C_{th}$ is given by

$$\Delta p_{V_{th}} = \frac{1}{2} \rho V_{th_R}^2 C_{th} \tag{1.13}$$

The total pressure drop in the reverse direction is given by

$$\Delta p_R = \Delta p_\theta + \Delta p_r + \Delta p_{V_{th}} = \frac{1}{2} \rho V_{th_R}{}^2 K_v^2 \tag{1.14}$$

where

$$K_v^2 = \frac{1}{A_R^2}\left(1 - \left(\frac{r_i}{r_v}\right)^2\right) + V_{tr}^2\left(\left(\frac{r_v}{r_i}\right)^2 - 1\right) + C_{th} \tag{1.15}$$

and

$$V_{th_R} = \frac{\sqrt{\frac{2\Delta p_R}{\rho}}}{K_v} \tag{1.16}$$

The forward flow pressure drop is given by

$$\Delta p_F = \frac{1}{2} \rho V_{o_F}{}^2 = \frac{1}{2} \rho \left(\frac{V_{th_F}}{A_R}\right)^2 \tag{1.17}$$

or

$$V_{th_F} = A_R\sqrt{\frac{2\Delta p_F}{\rho}} \tag{1.18}$$

The diodicity of the valve is then determined from the mass flow ratio

$$D_v = \frac{\dot{m}_F}{\dot{m}_R} = \frac{V_{th_F}}{V_{th_R}} = \frac{A_R\sqrt{\frac{2\Delta p_F}{\rho}}}{\frac{1}{K_v}\sqrt{\frac{2\Delta p_R}{\rho}}} = A_R K_v \tag{1.19}$$

because diodicity is defined as the mass flow ratio at equal pressure drop or $\Delta p_F = \Delta p_R$.

GEOMETRY CONSIDERATIONS

**Figure 5** shows all geometry parameters which are relative to the vortex aerovalve. In the current method of theoretical performance development the parameters $r_v/r_o$, $L_n$ and N are chosen as inputs and the remainder of the parameters are calculated from them. The values for $c_f$ and $c_{th}$ are chosen arbitrarily and their effect will be investigated through experimentation. The angle $\theta$ has been set equal to the angle $\alpha$ for two reasons. The unknown angle $\theta$ can be eliminated this way. Also, since it is observed from the geometry that

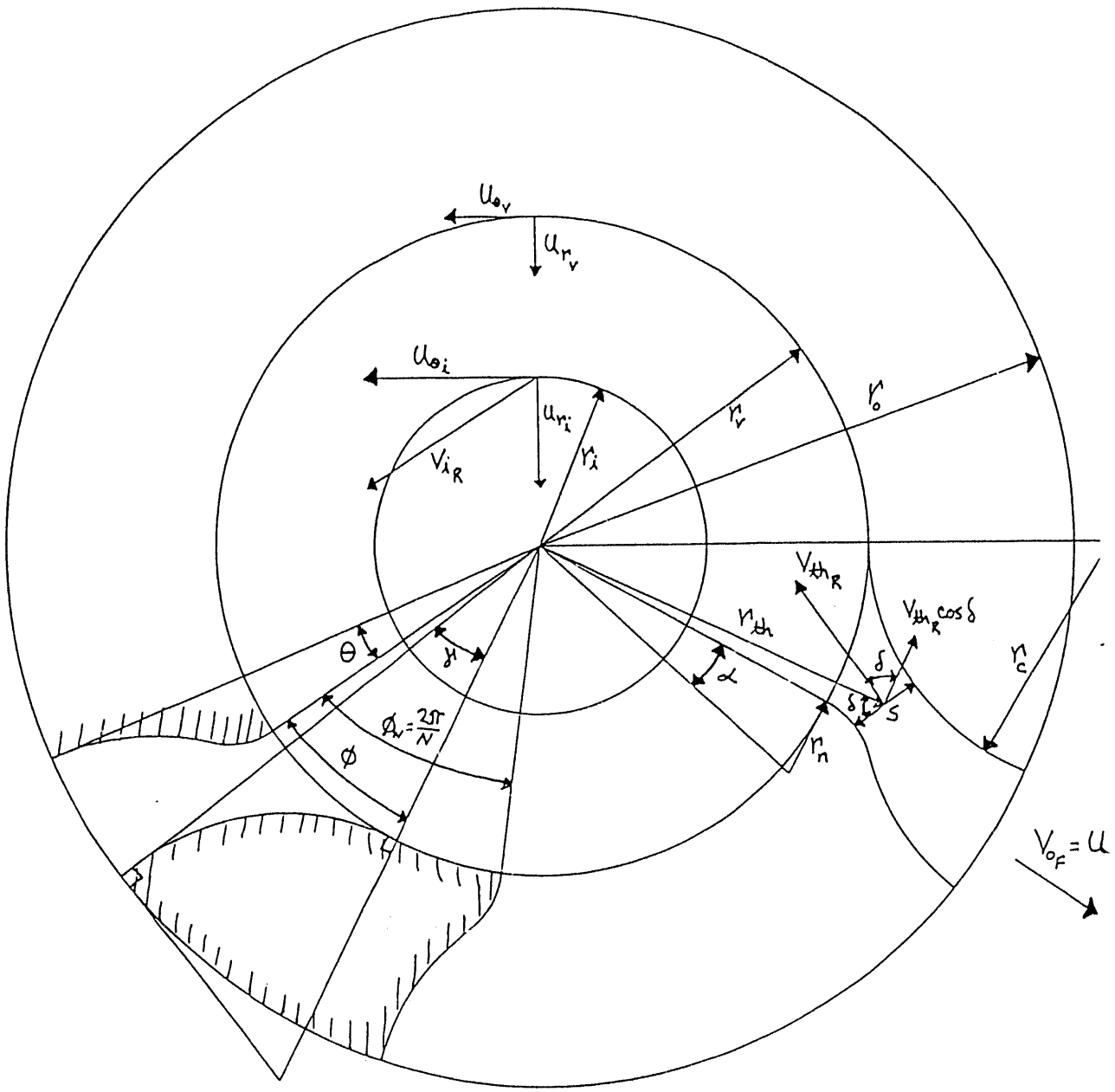


**FIGURE 5: FLOW AND GEOMETRY PARAMETERS USED IN THEORETICAL VORTEX AEROVALVE ANALYSIS**

$$\frac{r_n}{r_o}\cos\theta - \frac{r_v}{r_o}\cos\theta\tan(\alpha-\theta) + \frac{r_v}{r_o}\sin(\theta) + \frac{r_n}{r_o}\sin(\theta)\tan(\alpha-\theta) \quad (1.20)$$

and by rearranging

$$\tan(\theta) = \frac{\frac{r_n}{r_o} - \frac{r_v}{r_o}\tan(\alpha-\theta)}{\frac{r_v}{r_o}\left(1 + \frac{r_n}{r_v}\tan(\alpha-\theta)\right)} \quad (1.21)$$

Dividing by $r_v / r_o$ and noting that $\tan\alpha = r_n / r_v$ gives

$$\tan(\theta) = \frac{\tan(\alpha) - \tan(\alpha-\theta)}{1 + \tan(\alpha)\tan(\alpha-\theta)} \quad (1.22)$$

The right side of Equation 1.22 is of the form of the trigonometric identity

$$\tan(a-b) = \frac{\tan(a) - \tan(b)}{1 + \tan(a)\tan(b)} \quad (1.23)$$

with a = $\alpha$ and b = $(\alpha-\theta)$. It follows that for $\tan(\theta)$ to be equal to $\tan(\alpha-(\alpha-\theta))$ in terms of the two angles, the angles $\theta$ and $\alpha$ must be equal. Geometrically, from Figure 5 it is seen that the angle $\alpha$ must occur in the range $0 < \alpha < 90^\circ$ and $\theta < \gamma$.

Another consideration is the determination of the inlet radius $r_i / r_o$. To allow for the testing of several different valve configurations with a minimum amount of construction, the inlet radius is calculated by setting

$$2\pi r_i s = \frac{4}{N}(A_e - A_R N s^2) \quad or \quad r_i = \frac{4A_R s}{2\pi} \tag{1.24}$$

Note that $r_i$ / $r_o$ defined this way is the same for N = 1, 2, 3, and 4 throats.

THEORETICAL RESULTS

The results obtained from the computer program with the updated theory are shown in Figure 6. The graph is of $A_R$, $K_v$, $D_v$, and diffuser length to throat width ratio versus the vane inlet radius $r_v$ / $r_o$. The design throat width is s / $r_o$ = 0.1426 and the number of throats N = 4. The range of $r_v$ / $r_o$ is 0.4 to 0.7 and $A_R$ is limited to the range of 1.5 to 2.5. For these conditions $K_v$ ranges from 1.4 to about 2.5, $D_v$ from 3.2 to about 3.7, and the diffuser length to throat width ratio from 2.8 to about 1.9. It was decided from these curves to construct a valve for experimental purposes with the following parameters:

Outer radius $r_o$ = 3.5"

| | Non-dimensional | Dimensional | |
|---|---|---|---|
| N: | 4 | | |
| $r_c/r_o$: | 0.40205 | 1.41 Inches | $\phi$ : 26.00 degrees |
| $r_n/r_o$: | 0.1067 | 0.3733 Inches | $\beta$ : 37.78 degrees |
| $s/r_o$: | 0.1418 | 0.4962 Inches | $\theta$ : 8.910 degrees |
| $r_{th}/r_o$: | 0.7616 | 2.6657 Inches | $\gamma$ : 21.90 degrees |
| $r_v/r_o$: | 0.6800 | 2.3800 Inches | $\delta$ : 59.36 degrees |
| $r_i/r_o$: | 0.1446 | 0.5060 Inches | $\alpha$ : 8.910 degrees |

A drawing of the valve is shown in Figure 7. Construction of the valve itself and the test apparatus is currently underway.

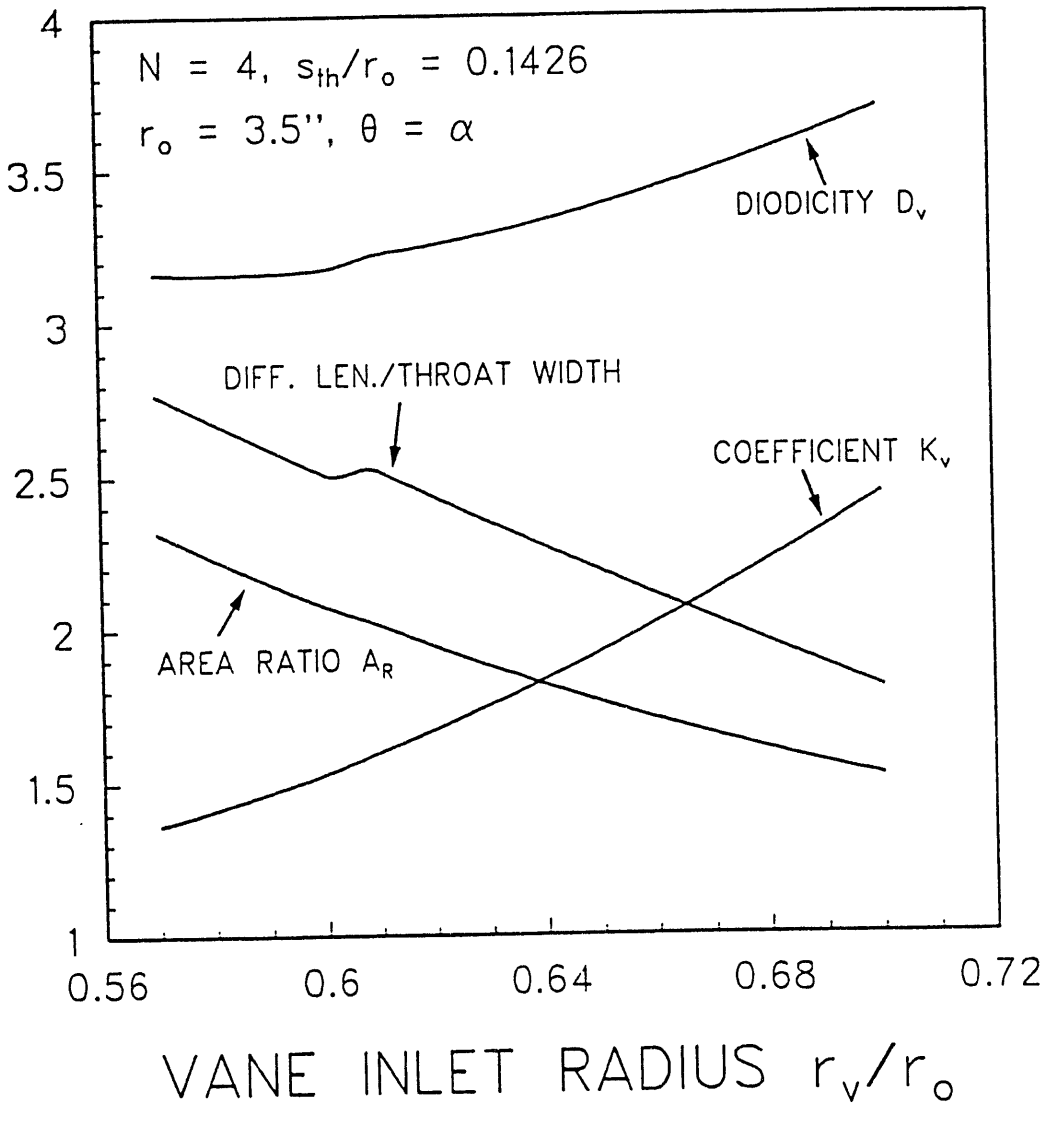


**FIGURE 6: PLOT OF VORTEX AEROVALVE THEORETICAL RESULTS FOR N = 4 THROATS**

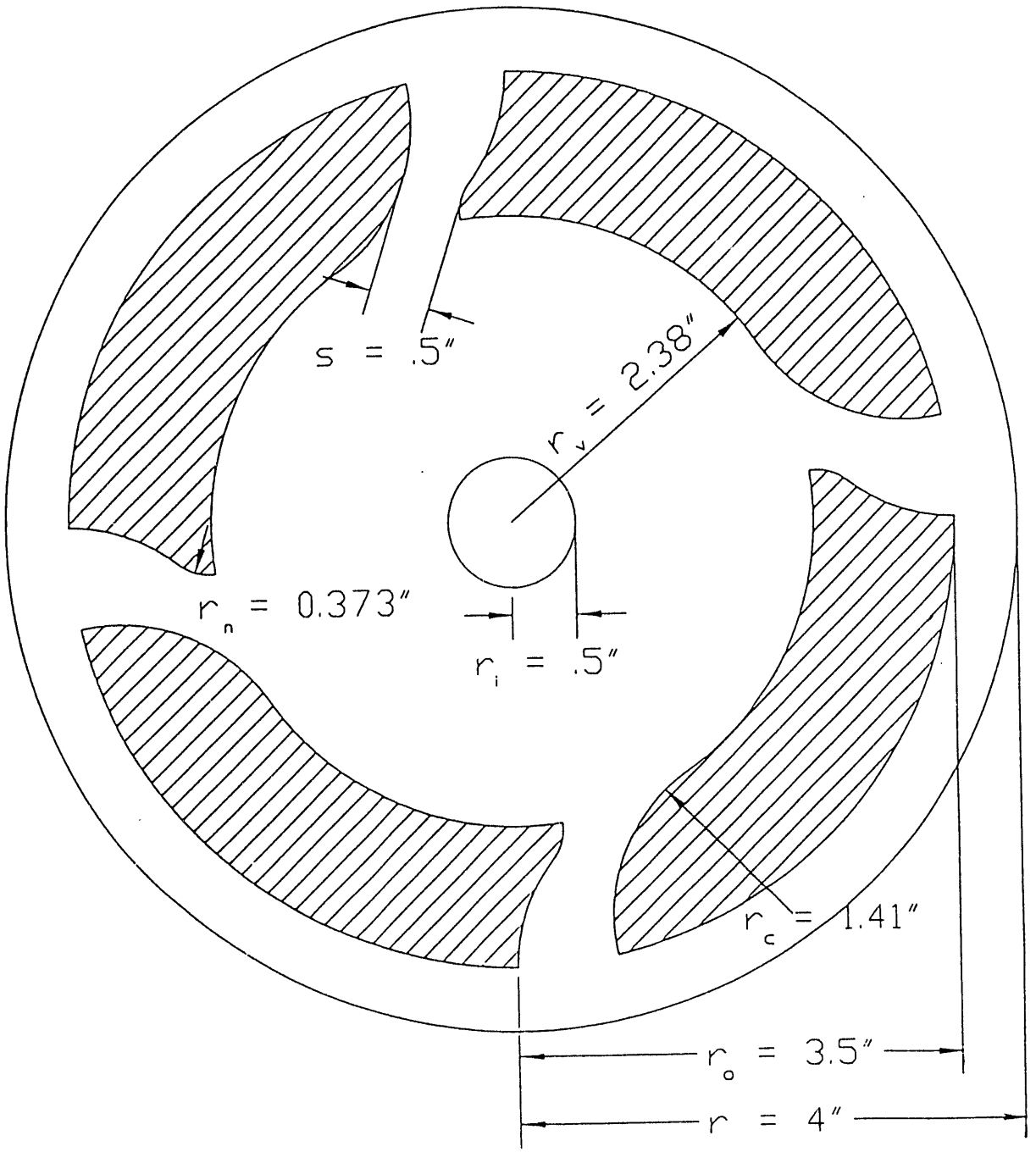


**FIGURE 7: EXPERIMENTAL CONFIGURATION WITH N = 1 TO 4 THROATS**

## 2.2.2 AEROVALVE FABRICATION

CONSTRUCTION OF VORTEX AEROVALVE AND STEADY FLOW TEST APPARATUS

Construction of the vortex aerovalve described in the previous subsection report was completed and work on the steady flow test apparatus was started. The apparatus is shown in Figure 8. The two flanged plexiglass columns are bolted together with a distributor plate between the flanges. High pressure air is admitted to the lower column and is distributed as it passes through the plate. The air then enters the valve, which is bolted to the flange on the top of the column. Both the forward and reverse flow tests are performed by simply connecting the valve in the proper configuration. Mass flow rate is measured before the air enters the lower column using a mass flow meter and pressures are measured using mercury and water manometers.

NOMENCLATURE

$A_{in}$ = cylindrical inlet area ($2 \pi r_i s$), taken equal to $A_o$

$A_o$ = the forward flow total exit area at $r_o$

$A_{th}$ = the sum of the throat areas ($N s^2$)

$A_R$ = vane exit to throat area ratio

$D_v$ = diodicity, forward to reverse mass flow ratio at same $\Delta p$

$K_v$ = coefficient which accounts for vortex contribution to valve diodicity

$L_n$ = percent of nose radius in ($r_o - r_v$)

$p_{(\ )}$ = pressure, the subscript t indicates total pressure, other subscripts indicate location based on radii subscripts

$\Delta p$ = static pressure differential

$\Delta p_F$ = between stagnation inlet condition and outlet $p_o$ at $r_o$ in forward flow

$\Delta p_R$ = between stagnation chamber conditions at $r_o$ and outlet $p_i$ at $r_i$ in reverse flow

$\Delta p_{th}$ = reverse flow pressure drop inside vane until flow separation at throat

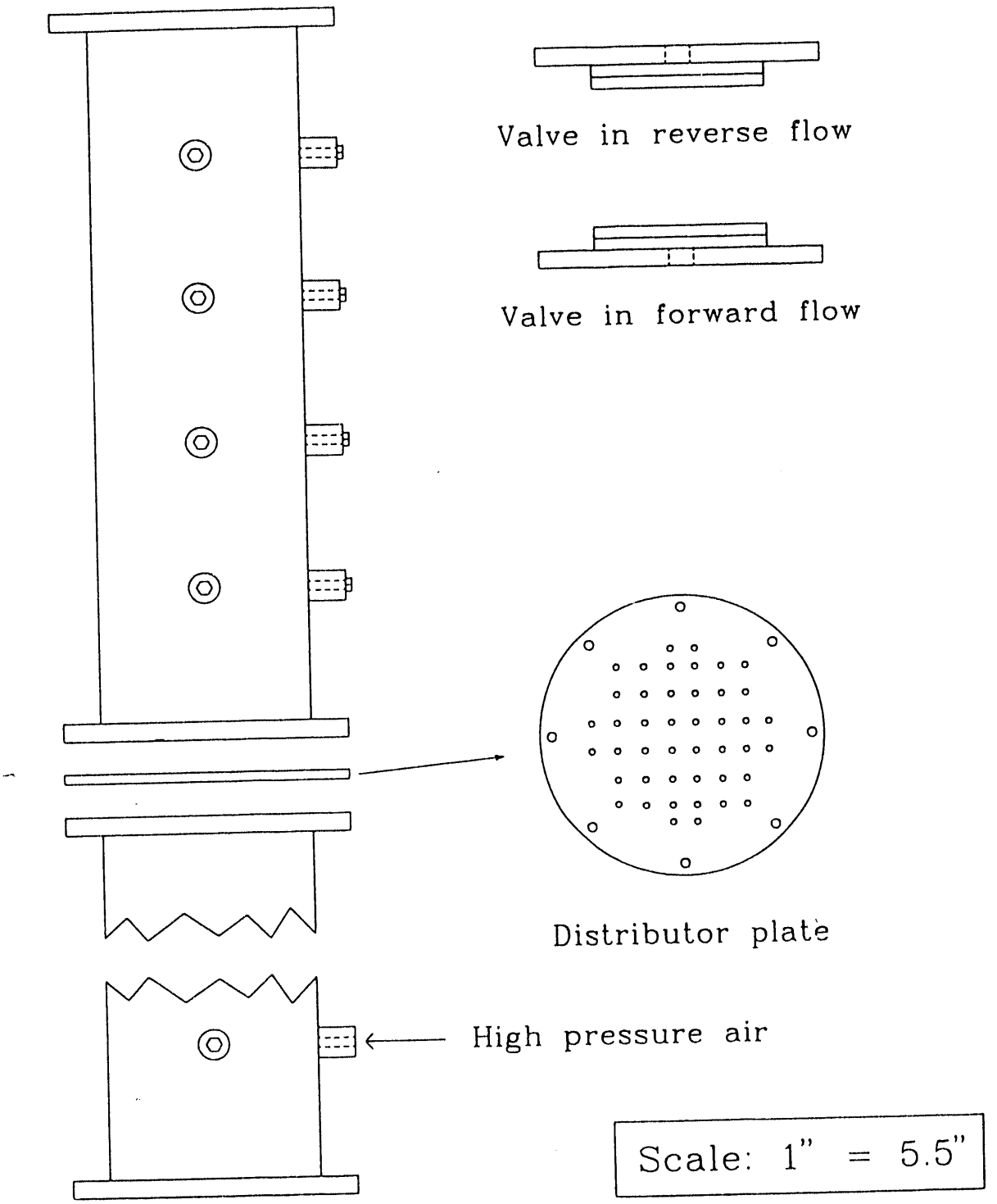


**FIGURE 8: PLOT OF VORTEX AEROVALVE RESULTS FOR N = 2 THROATS**

$\Delta p_\theta$ = curved flow pressure drop inside the vortex with reverse flow

$\Delta p_r$ = radial flow diffusion with reverse flow and re-separation at $r_i$

$r_{(\ )}$ = radius with subscript identifying location

s = throat width and depth

U = velocity component in the radial (r) and tangential ($\theta$) directions

V = velocity vector, subscript indicates location and subscript (F) used for forward flow and subscript (R) used for reverse flow

Subscripts

F = forward flow

R = reverse flow

fr = friction ratio

$\theta$ = tangential direction

r = radial direction

i = forward flow inlet

e = forward flow exit

o = vane outer radius

c = vane radius

n = vane nose radius

th = vane throat

v = vane inlet radius, or vortex

i = inlet duct radius

Geometry Angles

$\alpha$ = angle between center of nose radius arc and vane inlet

$\beta$ = angle between vane exit and inflection point of the vane curve

$\gamma$ = angle between top vane surface at vane exit and next vane inlet

$\delta$ = angle between throat width, s, and throat radius $r_{th}$

$\theta$ = vane pitch angle

$\phi$ = vane inlet spacing angle

## 2.3 FUNDAMENTAL SORBENT STUDIES (PENN STATE UNIVERSITY)

The objective of Task 1 is to conduct a fundamental study of the physical and chemical changes that calcium-based sorbents undergo when subjected to high heating rates for short residence times. Specifically, the aim is to determine if a flash calcination phenomenon occurs and if so whether it produces a calcine which is highly reactive on subsequent sulfation.

The objective of Task 2 is to conduct a two-stage fundamental study of the bimodal acoustic agglomeration of fly ash and sorbent particles. In the first stage, an entrained-flow reactor (EFR) will be used to optimize the frequency and sound pressure level for a range of fly ash and sorbent mass loadings, particle sizes and reactor temperatures. The focus of the experiments in the second stage of the agglomeration investigation will be to identify experimentally the mechanisms that control the bimodal agglomeration and cohesion of fly ash and sorbent particles under the influence of a high intensity acoustic field.

In Task 3, the results from the two fundamental studies (i.e., Tasks 1 and 2) will be combined into one model to predict sulfur capture and bimodal acoustic agglomeration under pulse combustion conditions. As experimental data become available from Tasks 1 and 2, progress on Task 3 will be reported.

### 2.3.1 TASK 1: FUNDAMENTAL STUDY OF SORBENT BEHAVIOR

The gas temperature at various locations within the reactor for different preheat temperatures was remeasured using a newly designed suction pyrometer design. The suction pyrometer was redesigned to increase the shielding of the thermocouple from the radiation in the reactor. Reactor temperature profiles were determined for preheat temperatures of 900, 1000 and 1100°C. Temperatures were measured at the injector tip and along the isothermal zone of the reactor. The reactor temperature profiles as a function of preheat temperature are shown in Figure 9. The relationship between gas temperature and reactor wall temperature was also determined and is shown in Figure 10.

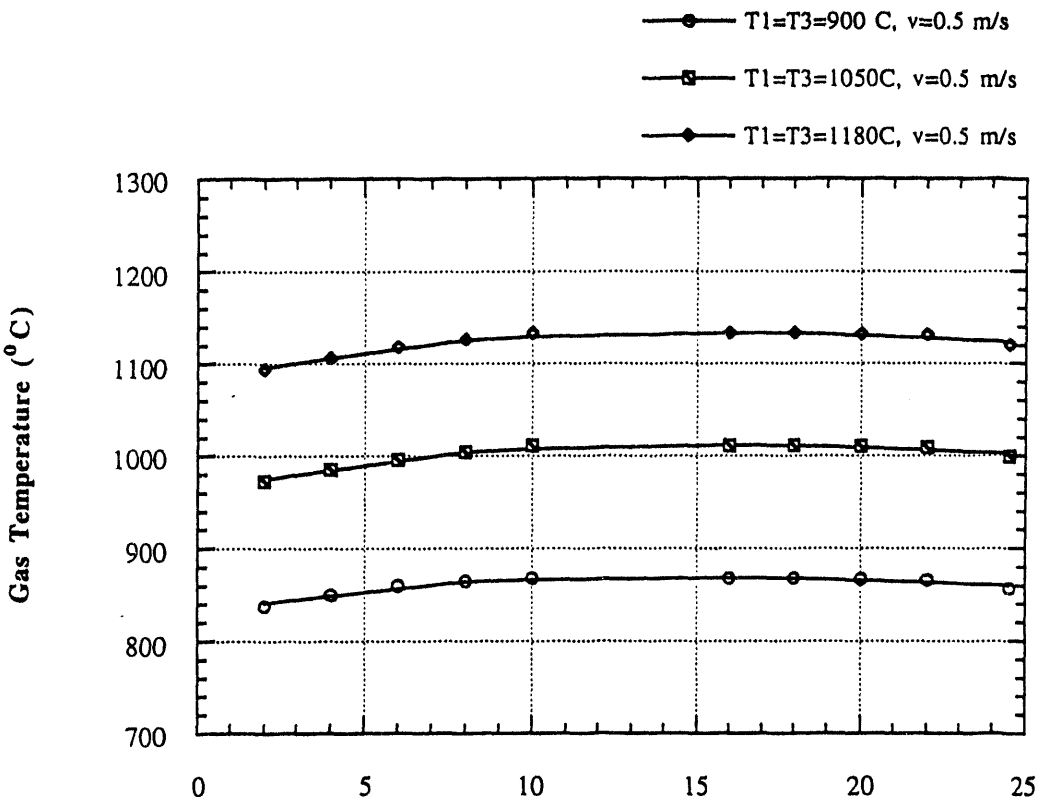


**FIGURE 9: GAS TEMPERATURE PROFILE FOR VARIOUS PREHEAT TEMPERATURES**

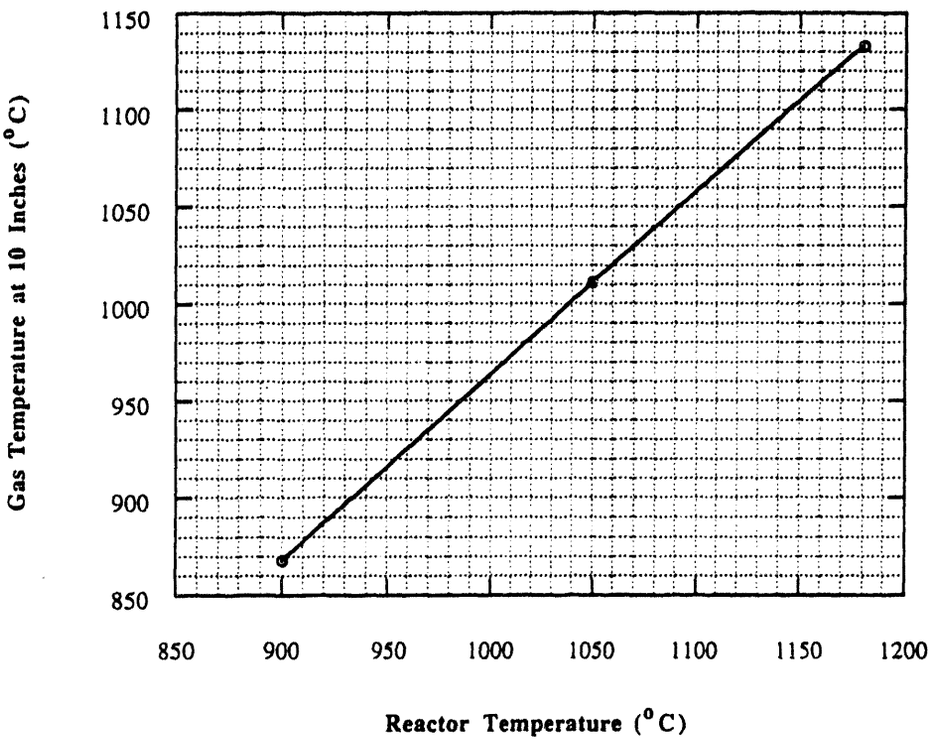


**FIGURE 10: RELATIONSHIP BETWEEN GAS TEMPERATURE AND REACTOR WALL TEMPERATURE**

Preliminary results of calcination tests performed in the entrained flow reactor were presented in the previous Quarterly report. The extent of calcination for three sorbents (Linden Hall, Bossardville, and Nittany) for three different particle sizes (45, 63, and 89 $\mu$m), tested at two reactor temperatures (1000 and 1100°C) were reported. For all three particle size of all three sorbents the extent of calcination at a given location in the reactor increased upon increasing the reactor temperature from 1000 to 1100°C. In addition, the extent of calcination was inversely related to particle size.

Upon closer examination of the data, an inconsistency was noted in the relationship between particle size and the extent of calcination. At the first sampling site in the reactor, approximately 4 inches from the injector tip, larger particles were calcined to a greater extent than smaller particles. One concern was that the sample probe was not sufficiently quenching the larger particles to halt the calcination process. The larger particles have a greater mass and cool slower than the smaller particles within the probe; therefore, the possibility that the larger particles continue to calcine within the probe was of concern. Modifications were made to the sample probe to improve its quenching capabilities. This included the addition of a nitrogen purge.

In addition, it was discovered that the type of wire used for the thermocouples in the newly remodeled entrained flow reactor was inappropriate. The preheat temperatures measured during the first set of calcination tests were actually much lower than the 1000 and 1100°C reported. The lower preheat temperature reduced the extent to which the sorbents were calcined.

It is therefore recommended that the calcination data presented in the July-September Quarterly report should be disregarded. Repeated calcination tests were conducted using the new probe design and the rewired thermocouples. Results of these tests are given in Table 2. Figures 11 through 13 show the extent of calcination for the three sorbents as a function of temperature, particle size, and distance along the reactor.

## TABLE 2:
## CALCINATION DATA FOR THE TEST SORBENTS

(values given represent the mass percent of sorbent calcined)

| DISTANCE FROM INJECTOR (in.) | SORBENT/GAS TEMPERATURE | | | | | |
|---|---|---|---|---|---|---|
| | Linden Hall | | Bossardville | | Nittany | |
| | 1000°C | 1100°C | 1000°C | 1100°C | 1000°C | 1100°C |
| | **Particle Size - 45 μm** | | | | | |
| 4 | 4.92 | 10.61 | 4.78 | 11.03 | 16.30 | 20.10 |
| 7 | - | 26.40 | - | 26.87 | - | 42.12 |
| 10 | 20.56 | 46.10 | 20.92 | 48.16 | 37.39 | 58.58 |
| 14 | - | 72.19 | 52.15 | 72.83 | 62.11 | 80.30 |
| 18 | 67.14 | 88.82 | 74.25 | 95.03 | 81.89 | 95.08 |
| 22 | - | - | 84.07 | - | 89.37 | - |
| 24 | 86.98 | 96.81 | 91.58 | 97.86 | 92.64 | 97.08 |
| | **Particle Size - 63 μm** | | | | | |
| 4 | 5.58 | 8.84 | 3.85 | 7.27 | 15.49 | 14.73 |
| 7 | - | - | - | - | - | - |
| 10 | 20.60 | 37.52 | 20.61 | 49.98 | 34.79 | 55.67 |
| 14 | 51.69 | - | - | - | - | - |
| 18 | 65.14 | 83.56 | 70.96 | 92.46 | 73.37 | 93.75 |
| 22 | 80.48 | - | - | - | - | - |
| 24 | 82.95 | 94.98 | 88.81 | 97.97 | 91.13 | 96.29 |
| | **Particle Size - 89 μm** | | | | | |
| 4 | 3.85 | 4.39 | 4.08 | 7.10 | 13.06 | 16.05 |
| 7 | - | - | - | - | - | - |
| 10 | 16.17 | 35.17 | 22.31 | 43.48 | 33.85 | 59.24 |
| 14 | - | - | - | - | - | - |
| 18 | 62.08 | 84.86 | 66.59 | 90.44 | 77.96 | 94.05 |
| 22 | - | - | - | - | - | - |
| 24 | 80.27 | 95.32 | 85.19 | 97.94 | 91.08 | 97.31 |

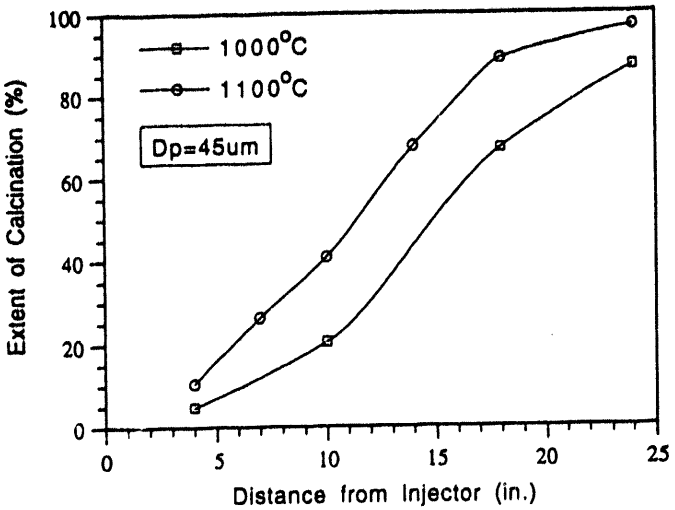


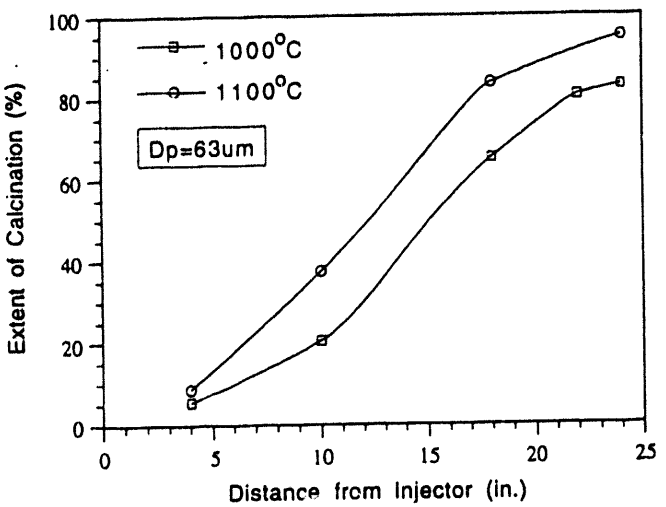


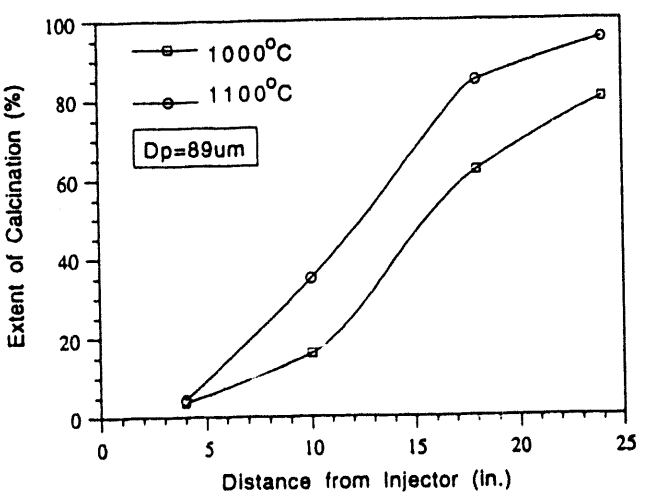


**FIGURE 11: CALCINATION PROFILES FOR THE THE LINDEN HALL SORBENT**

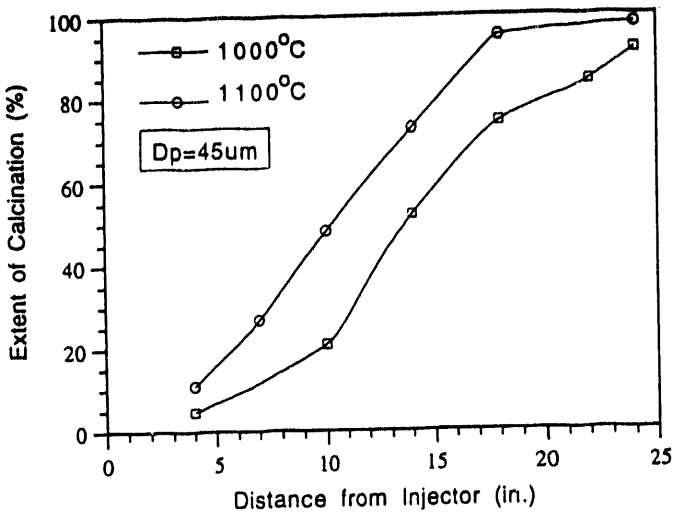


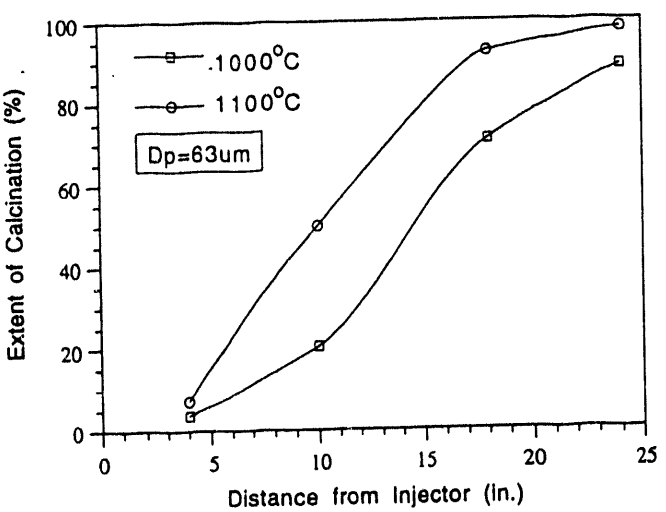


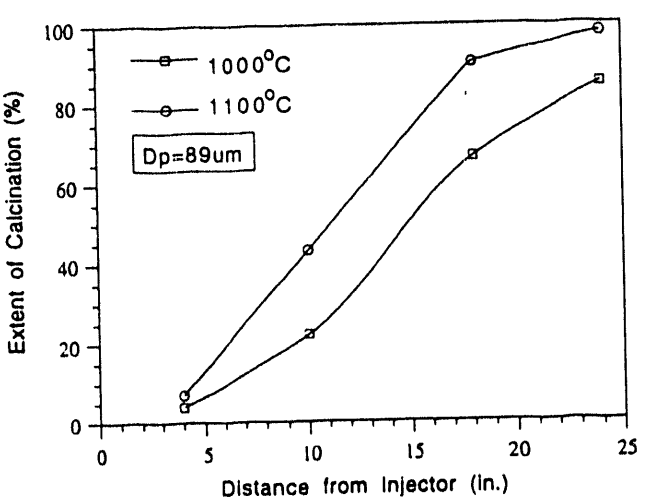


**FIGURE 12: CALCINATION PROFILES FOR THE BOSSARDVILLE SORBENT**

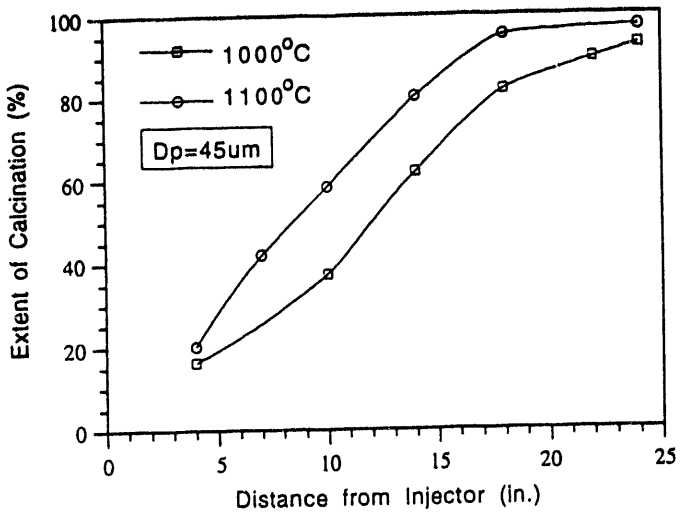


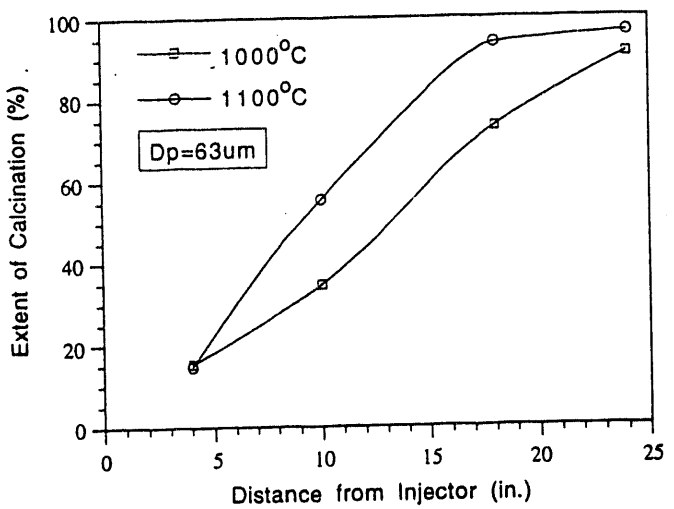


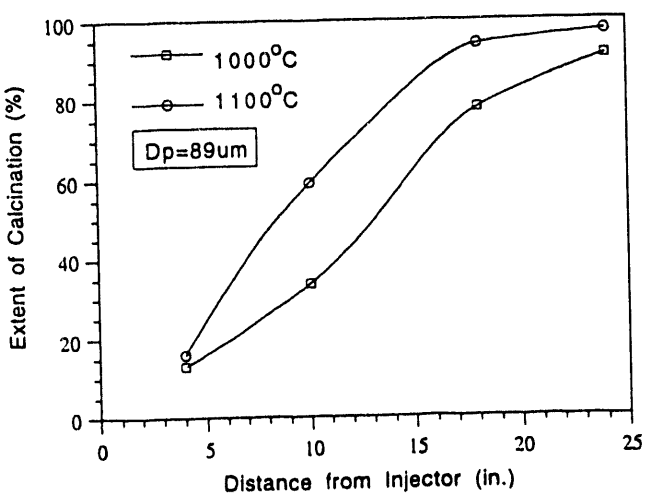


**FIGURE 13: CALCINATION PROFILES FOR THE NITTANY DOLOSTONE**

Sulfation tests without acoustic enhancement were conducted on the Linden Hall, Bossardville, and Nittany stones. Three size ranges of particles of each stone were tested. The particle size ranges were 37-53, 53-74, 74-105 μm (mean particle size of 45, 63, and 89 μm), tested at two reactor temperatures - 1000°C and 1100°C. The test conditions for the sulfation studies were the same as those used in the calcination tests report in the October 1993 monthly report. Sulfur dioxide was injected into the reactor during the tests at a concentration of 2000 ppmv. A S:Ca molar ratio of 0.5 was used in each test.

Samples collected at the various locations using a nitrogen-purged, water-cooled sampling probe. Samples were analyzed for sulfur to determine the extent of sulfur capture. The S:Ca molar ratios for the various samples are given in Tables 3 through 5. The data are shown graphically for the three size fractions at 1000°C and 1100°C for the Linden Hall, Bossardville, and Nittany stones in Figures 14 through 16.

Temperature Effects. In general, an increase in reactor temperature results in an increase in sulfur capture by all three sorbents throughout the reactor. However, the greatest increase in sulfur capture due to increased temperature is observed in the samples collected in the mid-section of the reactor, i.e., 10 inches from the point of sorbent injection.

Particle Size Effects. Larger particles captured less sulfur on a calcium molar basis than smaller particles. This agrees with earlier conclusions that the extent of calcination and subsequent sulfation of a sorbent is increased when particle size is reduced. The Nittany Dolostone showed the least reduction in sulfur capture due to increased particle size. A reduction of 9.5% in the S:Ca molar ratio was observed for the Nittany Dolostone.

Further discussion and comparison of the results of the calcination and sulfation tests is given in a paper entitled "Experimental Investigation of High-Temperature, Short Residence-Time Calcination and Sulfation of Limestone and

## TABLE 3:
## LINDEN HALL SULFATION TEST RESULTS

| Location (inches) | 1,000°C Size (µm) | | | 1,100°C Size (µm) | | |
|---|---|---|---|---|---|---|
| | 45 | 63 | 89 | 45 | 63 | 89 |
| 4 | 0.007 | 0.006 | 0.007 | 0.010 | 0.007 | 0.010 |
| 7 | | | | 0.027 | | |
| 10 | 0.021 | 0.016 | 0.016 | 0.045 | 0.033 | 0.038 |
| 14 | | 0.036 | | | | |
| 18 | 0.068 | 0.055 | 0.050 | 0.077 | 0.070 | 0.069 |
| 22 | | 0.072 | | | | |
| 24 | 0.088 | 0.081 | 0.066 | 0.097 | 0.088 | 0.082 |

## TABLE 4:
## BOSSARDVILLE SULFATION TEST RESULTS

| Location (inches) | 1,000°C Size (µm) | | | 1,100°C Size (µm) | | |
|---|---|---|---|---|---|---|
| | 45 | 63 | 89 | 45 | 63 | 89 |
| 4 | 0.011 | 0.010 | 0.008 | 0.012 | 0.011 | 0.012 |
| 7 | | | | 0.030 | | |
| 10 | 0.026 | 0.024 | 0.025 | 0.054 | 0.053 | 0.051 |
| 14 | 0.050 | | | | | |
| 18 | 0.083 | 0.075 | 0.067 | 0.110 | 0.087 | 0.083 |
| 22 | | | | | | |
| 24 | 0.112 | 0.100 | 0.087 | 0.120 | 0.089 | 0.082 |

## TABLE 5:
## NITTANY SULFATION TEST RESULTS

| Location (inches) | 1,000°C Size (µm) | | | 1,100°C Size (µm) | | |
|---|---|---|---|---|---|---|
| | 45 | 63 | 89 | 45 | 63 | 89 |
| 4 | 0.046 | 0.047 | 0.037 | 0.044 | 0.024 | 0.037 |
| 7 | | | | 0.096 | | |
| 10 | 0.072 | 0.065 | 0.070 | 0.146 | 0.124 | 0.121 |
| 14 | 0.130 | | | | | |
| 18 | 0.217 | 0.201 | 0.166 | 0.257 | 0.235 | 0.233 |
| 22 | 0.260 | | | | | |
| 24 | 0.278 | 0.268 | 0.203 | 0.293 | 0.283 | 0.265 |

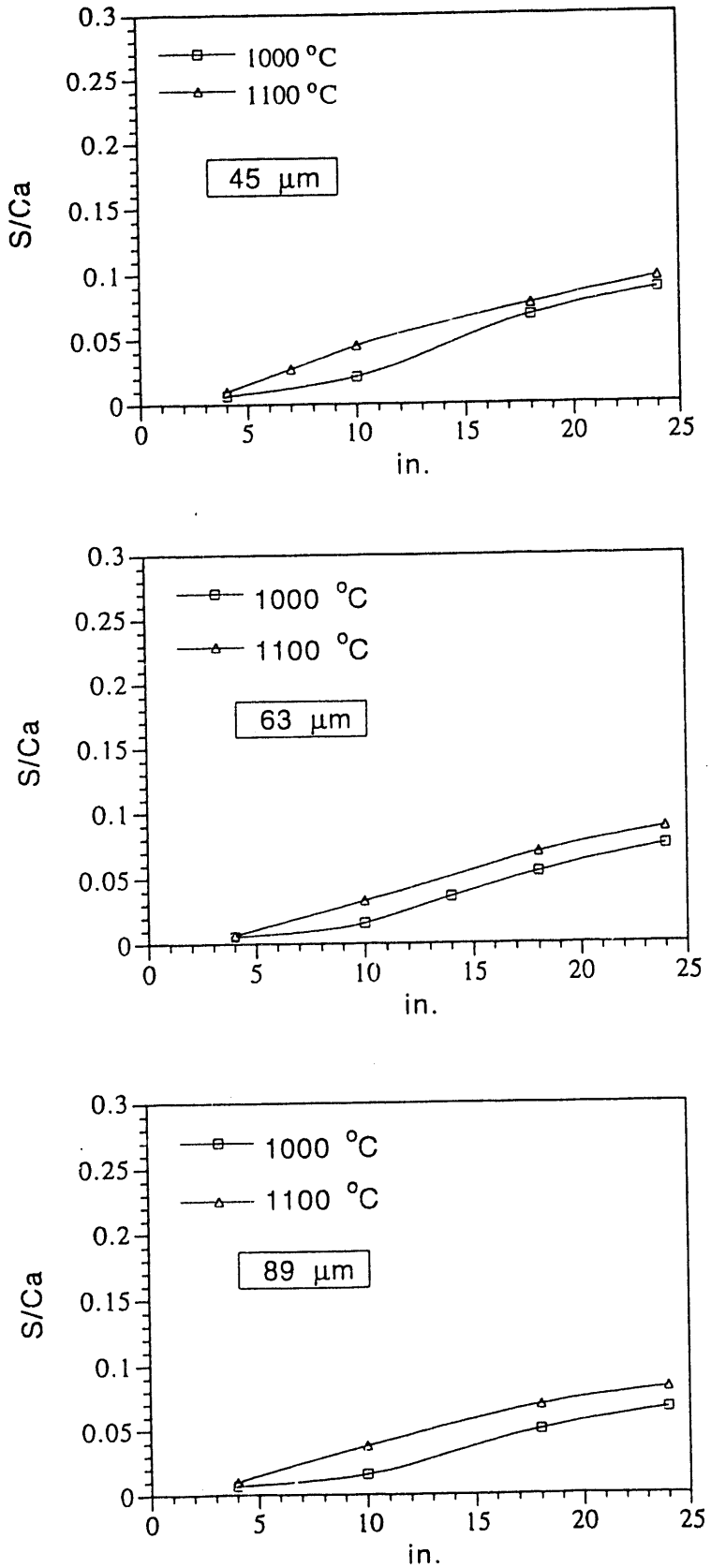


**FIGURE 14: RESULTS OF SULFATION TESTS CONDUCTED ON THE LINDEN HALL SORBENT**

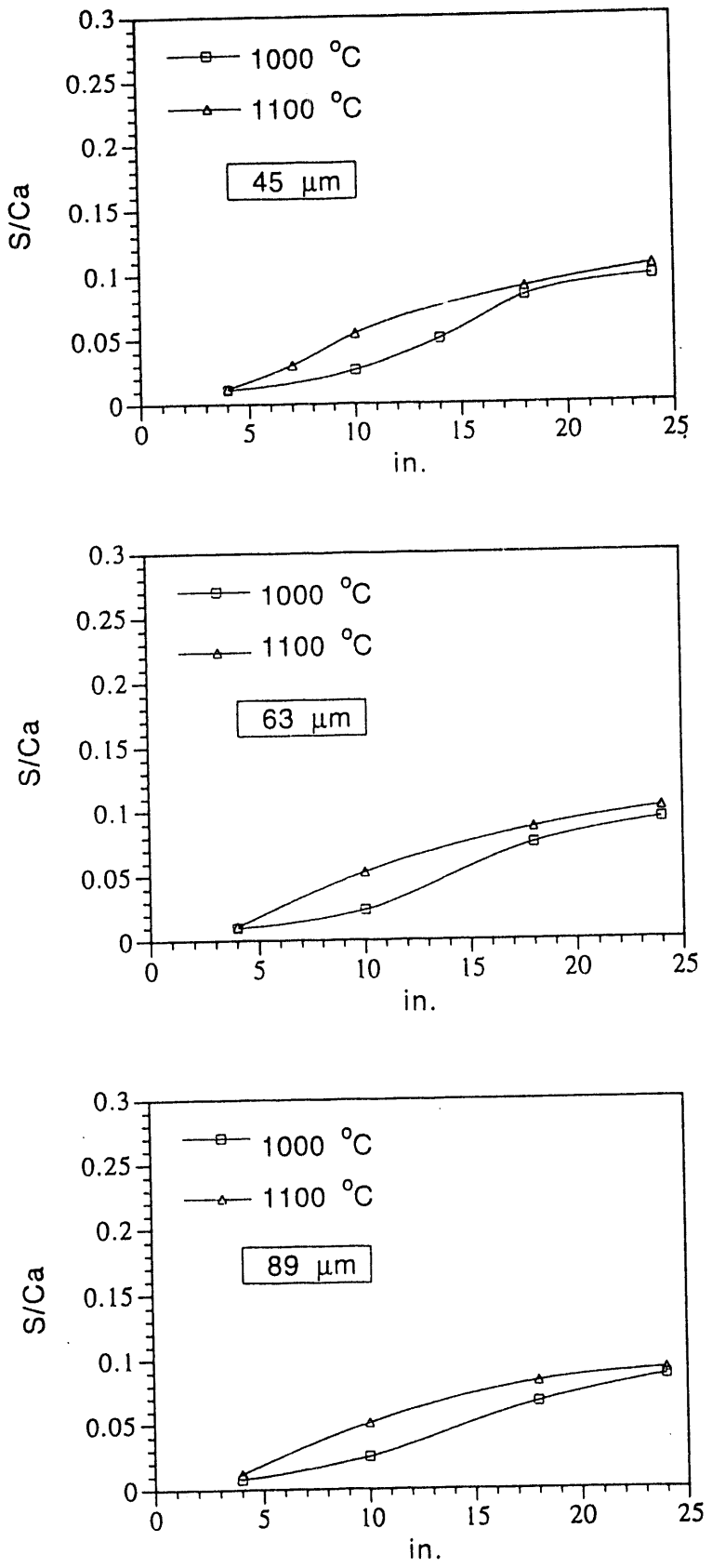


**FIGURE 15: RESULTS OF SULFATION TESTS CONDUCTED ON THE BOSSARDVILLE SORBENT**

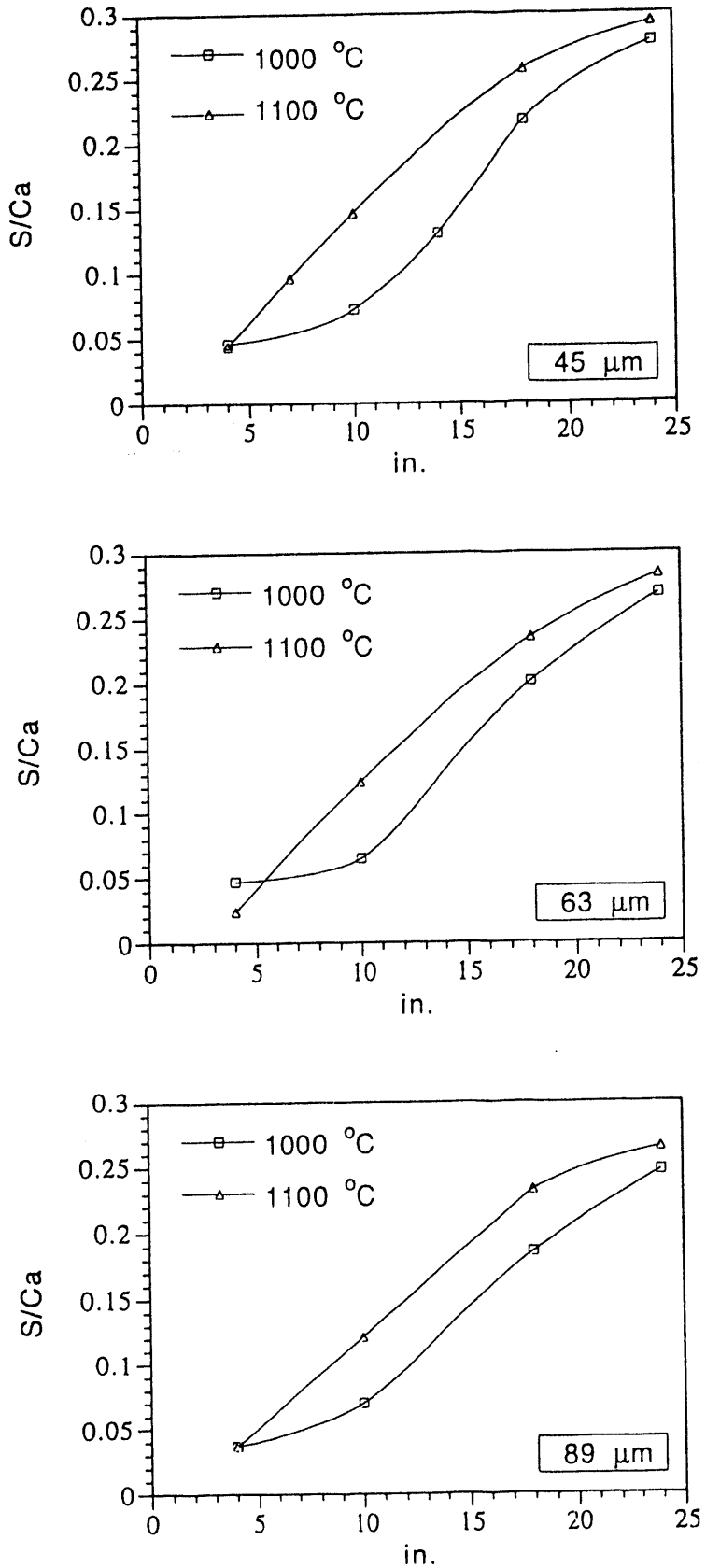


**FIGURE 16: RESULTS OF SULFATION TESTS CONDUCTED ON THE NITTANY SORBENT**

Dolostone Sorbents" submitted and accepted for the American Chemical Society National Meeting in San Diego, California, March 1994. A copy of the paper is included as Appendix A in this report.

Sulfation tests in the presence of an acoustic field will be conducted during the next period.

### 2.3.2 Task 2: Fundamental Study of Bimodal Acoustic Agglomeration

Statistical analysis of the baseline agglomeration tests conducted at ambient temperature with and without sound is still being conducted. The data are being evaluated to verify that the size distributions of the ash particles measured with and without sound represent two distinct particle populations.

### 2.3.3 Task 3: Sulfur Capture Model

It is well accepted that the effects of mass transfer, due to the imposition of an acoustic field, are more prominent in the case of larger particles (order of 100 $\mu$m) than for smaller particles. Figure 17 shows the variation in the Sherwood number with the acoustic intensity level, measured in decibels, within a field. Preliminary modeling runs were conducted to estimate the effect of an acoustic field on the rate of sulfation. Sulfation depends on many competing processes, namely, external heat and mass transfer from the surrounding gas to the particle, pore diffusion (a combination of bulk diffusion and Knudsen diffusion) from the surface of the particle to the interior, and product layer diffusion through the $CaSO_4$ formed on the individual grains as sulfation proceeds. It has been shown that smaller particles sulfate more quickly than larger particles. In the case of larger particles, the rates of pore diffusion and external heat and mass transfer are also more important in determining the rate of sulfation.

In the model it was assumed that individual limestone particles approximately 10 $\mu$m in size agglomerate to form 50, 100, or 200 $\mu$m particles when an acoustic field is applied (Figure 18). It follows that the larger agglomerate experiences increased mass transfer effects within the acoustic field during

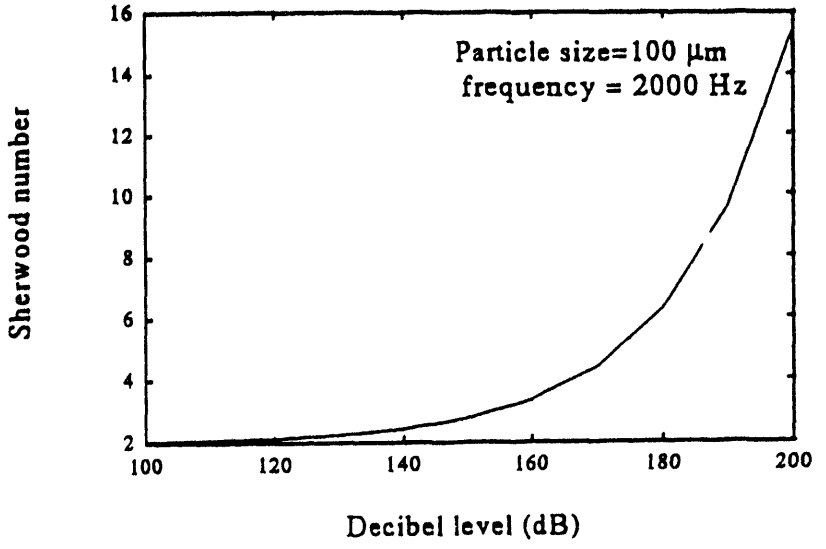


**FIGURE 17: RELATIONSHIP BETWEEN SHERWOOD NUMBER TO ACOUSTIC FIELD INTENSITY (dB)**

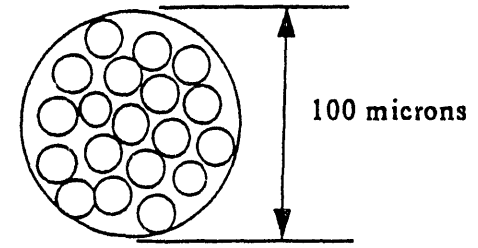


Agglomerated particle showing individual particles inside.

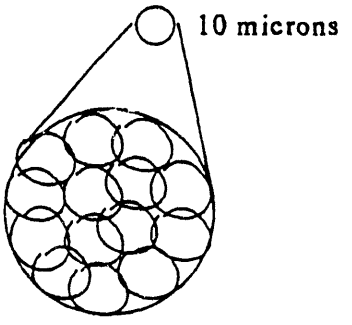


Expanded view of single particle showing individual grains which generally overlap.

**FIGURE 18: CONCEPTUAL VIEW OF AGGLOMERATE**

sulfation. The sulfation of the smaller particles is influenced primarily by product layer diffusion and pore diffusion. The result of applying an acoustic field is that the rate of sulfation of the particles within the agglomerate increases due to enhanced mass transfer of $SO_2$ to the calcine. Preliminary modeling results, presented in Figures 19 through 21, show the effect of increasing the acoustic field intensity (100 to 190 dB) on sulfur capture as a function of agglomerate size (50, 100, and 200 $\mu$m) and porosity (0.15, 0.35, and 0.50). The data suggest that for larger agglomerates the effect of the acoustic field intensity is greater than in the case of smaller agglomerates. In addition, the greater the porosity, the greater the extent of sulfur capture for the particle.

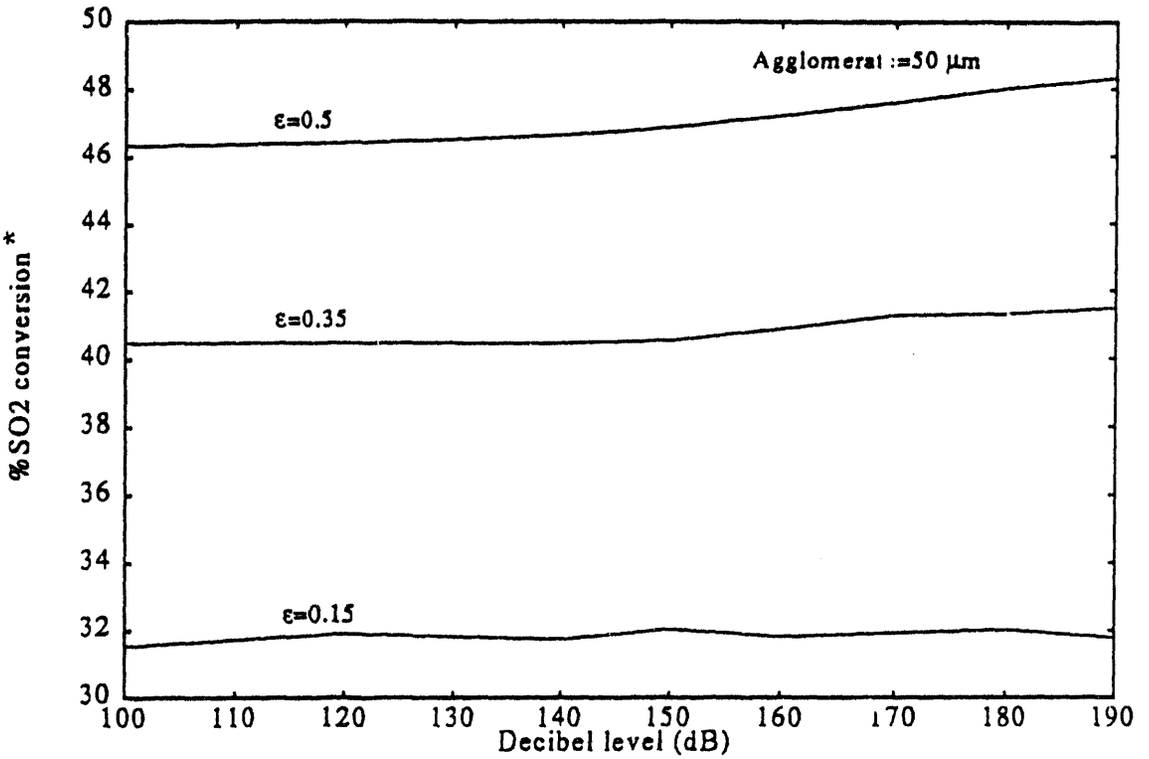


* $SO_2$ CAPTURE

**FIGURE 19: INFLUENCE OF AN ACOUSTIC FIELD ON $SO_2$ CAPTURE FOR A 50 µM LIMESTONE AGGLOMERATE ($\epsilon$ = POROSITY)**

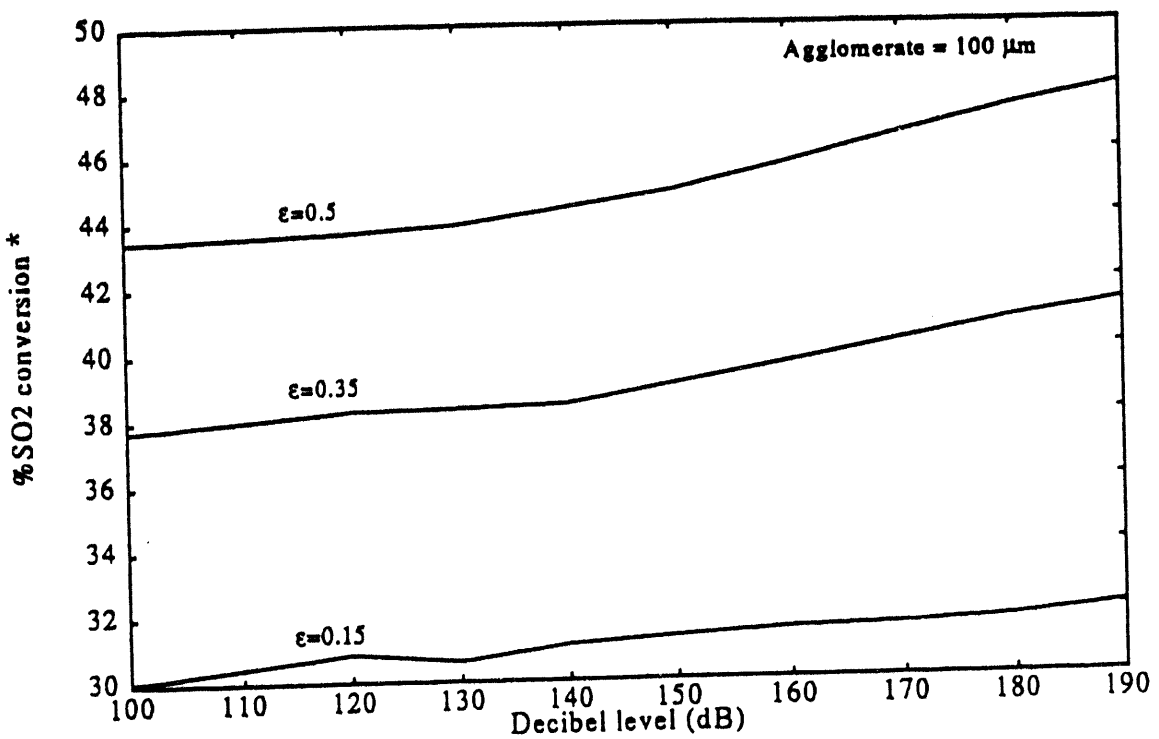


* $SO_2$ CAPTURE

**FIGURE 20: INFLUENCE OF AN ACOUSTIC FIELD ON $SO_2$ CAPTURE FOR A 100 µM LIMESTONE AGGLOMERATE ($\epsilon$ = POROSITY)**

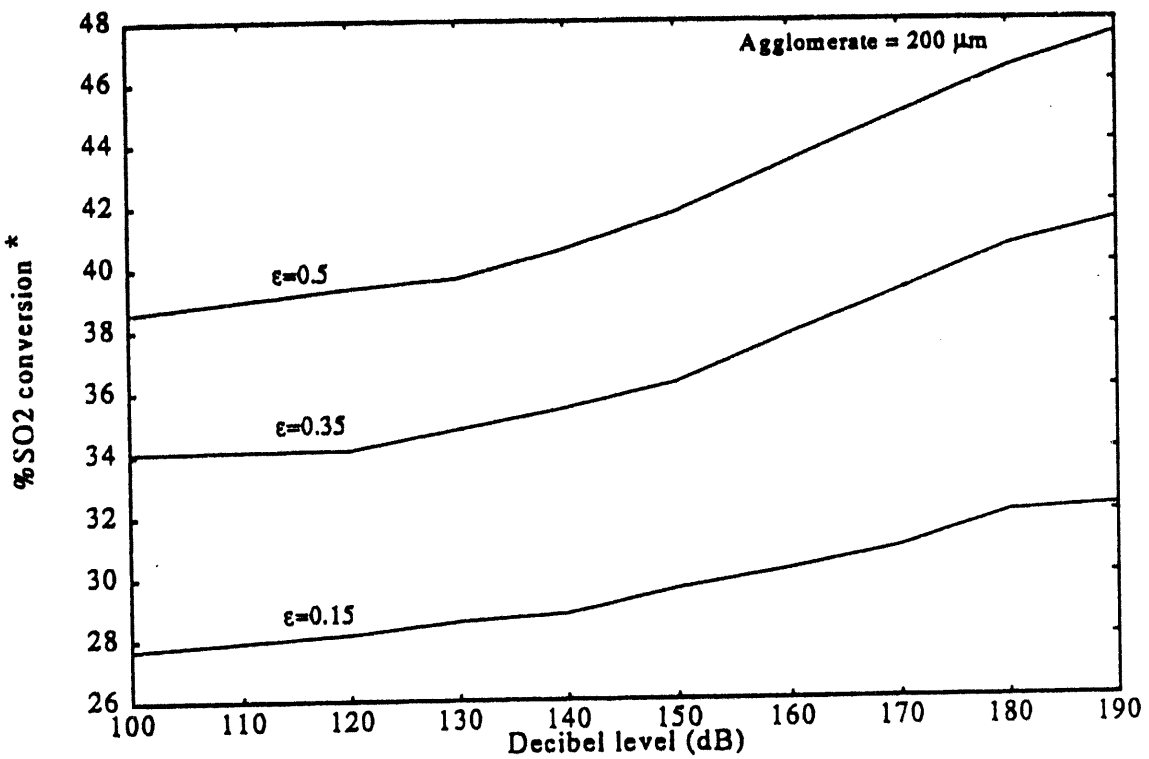


* $SO_2$ CAPTURE

**FIGURE 21: INFLUENCE OF AN ACOUSTIC FIELD ON $SO_2$ CAPTURE FOR A 200 μM LIMESTONE AGGLOMERATE (ε = POROSITY)**

# SECTION 3.0

## PLANS FOR NEXT PERIOD

- Fabricate and install a new isokinetic system.
- Calcine and classify lime for the bimodal test on the MTCI PAFBC unit.
- Perform tests on the bimodal unit.
- West Virginia University - Test the aerovalve fabricated.
- Penn State University - Complete data reduction.

# APPENDIX A

## (PENNSYLVANIA STATE UNIVERSITY)

# EXPERIMENTAL INVESTIGATION OF HIGH-TEMPERATURE, SHORT RESIDENCE-TIME CALCINATION AND SULFATION OF LIMESTONE AND DOLOSTONE SORBENTS

Naiyi Hu, Ye Liu, Sharon Falcone Miller and Alan W. Scaroni
The Pennsylvania State University
402 Academic Activities Building
University Park, PA 16802

Key words: sorbent furnace injection, calcination, sulfation.

## INTRODUCTION

Sulfur dioxide emissions from coal-fired utility boilers and furnaces continue to be of significant regulatory concern. One approach to reducing these emissions that has received considerable attention[1-4] is the injection of dry, pulverized sorbent (limestone or dolostone) into the combustion chamber. This technology has been applied to conventional coal-fired utility boilers[1,2] and is considered to be a good candidate for use in coal-fired heat engine applications.[3,4] During the process, the injected limestone or dolostone particles are rapidly heated by the hot combustion gases and calcined by the reactions $CaCO_3 \rightarrow CaO + CO_2$ and $CaMg(CO_3)_2 \rightarrow CaO + MgO + 2CO_2$, respectively. The CaO produced then reacts with $SO_2$ and excess $O_2$ in the combustion gases to form $CaSO_4$.

Experimental data on the rates of calcination, sintering and sulfation have been reported by Borgwardt and others.[5-8] The physical structure of the calcined sorbents has also been investigated,[5,9,10] and a number of models have been developed describing the calcination and sulfation processes.[10,11,12] The primary application of dry sorbent injection is to conventional coal-fired utility boilers. The sorbent particle size used is either small (in the range of 1 to 30 μm) in pulverized coal applications or large (in the range of 0.25 to 1 mm) for fluidized-bed applications. Few investigations have been carried out using 30 to 100 μm particles, which is the size range of interest for coal-fired heat engine applications.[3,4]

This study investigated the calcination and sulfation behavior of three different sorbents (two limestones and one dolostone) in the size range from 37 to 105 μm. The time required for heating and calcination, the effect of the calcination process on sulfation behavior, and the effect of sorbent type on sulfation behavior were of primary interest.

## EXPERIMENTAL

The calcination and sulfation experiments were conducted in the entrained-flow reactor illustrated in Figure 1. It consists of a preheater, a side-heated sorbent injector, and a vertical reactor. The preheater, injector and reactor were electrically heated to provide the desired gas preheating temperature and reactor temperature. The inside diameter of the ceramic reactor tube is 50.8 mm and it has an isothermal zone length of 600 mm. Dry air was used as the entrainment gas and was preheated to the same temperature as that in the reactor isothermal zone (±13 °C). The total gas flow rate was 60.7 l/min. As the preheated air passes through the injector section, the heat loss caused by contacting the injector wall is compensated for by the heat transferred from the heating wire wound around the outside of the injector. The sorbent was fed by a calibrated fluidized bed feeder. Room temperature air was used for sorbent injection and it comprised 5 % by mass of the total air flow to the reactor. A flow stabilizer was used to eliminate pulsations of the feed material caused by the fluidized feeder. $SO_2$ was doped into the gas flow by a mass flow controller to provide an $SO_2$ concentration of 2000 ppmv in the reactor. The sorbent feed rate was adjusted to achieve a Ca/S molar feed ratio of 2.0. Solid samples were collected through a nitrogen-purged, water-cooled sampling probe. During sampling, the nitrogen was used to increase the cooling rate of the sample. The nitrogen comprised 50 % of the total gas flow through

the probe. Calculations indicated that 89 μm particles were cooled from 1,100 to 700 °C within 0.03 second after entering the sampling probe.

The stratigraphic formations, chemical compositions and the specific BET surface areas of the two limestone and one dolostone sorbents tested are shown in Table 1. The materials were crushed and wet sieved to size fractions of 74-105 μm (140x200 US mesh), 53-74 μm (200x270 US mesh) and 37-53 μm (270x400 US mesh). The sieved materials were dried in an oven at 105 °C for 48 hours.

The solid samples extracted from the reactor were analyzed for loss-on-ignition (using a Leco MAC-400 proximate analyzer), BET surface area (using a Quantachrome Autosorb-1 analyzer system with nitrogen), and sulfur content (using a Leco SC-132 sulfur analyzer with $V_2O_5$ catalyst). Some hydration occurred during sample collection and transfer. The extent of hydration was determined (using the Leco MAC-400 proximate analyzer) and the calcination and sulfation data corrected accordingly.

## RESULTS AND DISCUSSION

### CALCINATION BEHAVIOR

The extents of calcination of the Linden Hall limestone at gas temperatures of 1,000 and 1,100 °C are shown in Figures 2 a and b, respectively. The initial calcination rate is slow, followed by a rapid increase and then a decline as the calcination process approaches completion. An initial slow rate of calcination was observed for all three sorbents studied and this was attributed to the use of ambient air as the injecting medium, and the time needed for the sorbent particles to reach their decomposition temperatures.

Effects of Ambient Air Sorbent Injection and Time Required for Particle Heating: Sorbent injection systems typically use ambient air as the injecting medium. To simulate this condition, the sorbents were entrained in air at room temperature. As previously indicated, the sorbent-entraining air comprised 5 %, by mass, of the total air flow to the reactor tube. This ambient air, when mixed with preheated air in the top of the reactor, reduced the reactor inlet temperature. Figure 3 shows the measured gas temperature profiles along the reactor. It was found that the gas temperature, at a location corresponding to 0.1 second after injection, was 40 °C lower than the gas temperature at the same location when no ambient air injection occurred. The lower inlet gas temperature caused by the ambient air injection resulted in a delay in the initial calcination of the sorbents.

Another reason for the significant delay in calcination was the heating time required for the relatively coarse sorbent particles to reach their decomposition temperature. Figure 4 shows the calculated temperature profiles of 10 and 63 μm particles as a consequence of convective heat transfer. It takes much longer for the relatively coarser sorbent particles (in the range of 37 to 105 μm) to heat up than for a 10 μm particle. The characteristic heating time for a 105 μm sorbent particle is 92 ms and that for a 10 μm sorbent particle is only 0.8 ms. This latter time is negligible for conventional utility boilers firing pulverized-coal where the effective sorbent reaction time is about 2 seconds. However, the characteristic heating time for 63 μm sorbent particles is 33 ms, which is significant in heat engine applications.

Effect of Sorbent Particle Size on the Calcination Process: Over the sorbent size range from 45 to 89 μm, the effect of particle size on the calcination process at 1,000 °C is shown in Figures 2 and 3. For the three sorbents studied, the extent of calcination was not significantly dependent on the sorbent particle size.

From the classical shrinking-core model, the extent of calcination can be expressed as:

$$x = 1 - ( 1 - k \cdot t / dp )^3 \qquad (1)$$

where dp is the particle diameter, k is the calcination rate constant and t is the calcination time. In Equation (1), the extent of calcination has a strong dependency on particle size. Borgwardt[5]

demonstrated that, when the resistances of intraparticle and interparticle mass transfer were eliminated, the calcination rate of small limestone particles could be described by a model that assumed a direct relationship with the specific BET surface area of $CaCO_3$. This calcination model has the form:

$$d(CaCO_3) / dt = k \cdot S_g \cdot (CaCO_3) \quad (2)$$

where $(CaCO_3)$ is the weight of the undecomposed carbonate and $S_g$ is the specific BET surface area of $CaCO_3$. By integration, the extent of calcination is related to the specific BET surface area by:

$$x = 1 - \exp ( - k \cdot t / S_g ) \quad (3)$$

Milne et al.[10] employed a modified shrinking-core model to interpret the experimental data of Borgwardt[5]. A good fit was obtained when the particle diameter dependency was reduced to the 0.6 power, and the empirically modified equation was:

$$x = 1 - ( 1 - k \cdot t / dp^{0.6} )^3 \quad (4)$$

Comparison of the calcination models with the experimental data for the Linden Hall limestone at 1,000 °C is shown in Figure 6. This data indicate that the calcination model based on the specific BET surface area of $CaCO_3$ is a better predictor of the experimental data than the modified shrinking core model. A comparison of the calcination models with the data for the Bossardsville and Nittany sorbents results in the same conclusion.

To be able to apply the modified shrinking-core model to the experimental data of this study requires that the particle size dependency be reduced to a power of between 0.2 to 0.3, depending on the particular sorbent. The very weak particle size dependency implies that these sorbents had very rough surfaces and the different size dependencies of the different sorbents may be related to the physical structures of the sorbents as well as to the chemical reactions that occur on the surface. This issue will be clarified in future studies.

## SULFATION BEHAVIOR

The sulfation data for the three sorbents at a gas temperature of 1,000 °C are shown in Figure 7. The extent of sulfation is expressed as the molar ratio of sulfur to calcium in the solid sample. The data reveal that the sulfation process for the limestone and dolostone particles in this size range was different than that associated with small particles (~5 μm) and precalcined sorbents.[13] There were no initial rapid sulfur capture periods as was the case for most small particles and precalcines.[13] The sulfation rates increased steadily and monotonically. In addition, the low calcium dolostone exhibited a greater sulfur capture capability than the high calcium limestone for the same experimental conditions. The 1,100 °C sulfation data for the three sorbents showed the same trends.

Effect of Calcination Rate on Sulfation Rate: Figure 8 shows the calcination and sulfation curves for 45 μm Bossardsville limestone particles at a gas temperature of 1,000 °C. The experimental data of Cole et al.[13] using precalcined limestone at similar sulfation conditions are also shown in Figure 8 (indicated by the square data points). Comparing the sulfation curves of the 45 μm limestone particles used in this study and that of Cole's study, the initial rapid sulfur capture period, typical of precalcines and small particles, was not apparent. Based on the calcination curves generated in this study, it is concluded that the delay in calcination is responsible for the initial lower extent of sulfur capture. For the 63 μm Bossardsville limestone particles, the extent of calcination was only 8 % for a 0.2 seconds particle residence time. Though the sulfation rate of the CaO produced was very high, there was not sufficient CaO available at that time for extensive sulfation to occur. As a consequence, the sulfur capture (based on the molar ratio of sulfur to calcium) was low. Despite the initial sulfation delay, the slope of the sulfation curve at longer residence times did not level off. The ongoing calcination proces ; produced fresh CaO surface to be sulfated. The production of a $CaSO_4$ layer from the CaO initially produced resulted in a slower

rate of sulfation due to product layer diffusion limitations. However, the sulfation rate of newly created CaO was rapid, thereby compensating for the slower rate of sulfation of the CaO beneath the $CaSO_4$ layer. For particle residence times up to one second, which corresponded to an 80 to 90 % extent of calcination, no significant decrease of the apparent sulfation rate was observed.

Effect of Sorbent Type on Sulfation: As shown in Figure 7, the different sorbents exhibited different sulfation performances at the same experimental conditions. For the sulfation tests with 45 μm particles at 1,000 °C and 1.1 second residence time, the calcium utilization of the Linden Hall limestone was 9 %, that of the Bossardsville limestone was 12 %, while that of the Nittany dolostone was 28 %. On the basis of sorbent utilization (rather than calcium utilization), the performance of the lower purity Bossardsville limestone was not significantly different than that of the high purity Linden Hall limestone. The Nittany dolostone, which contained only 50 % calcium carbonate, displayed better performance than the high purity Linden Hall limestone. At a Ca/S molar feed ratio of 2.0, the 45 μm Nittany dolostone particles reduced the $SO_2$ in combustion gas by 56 % in 1.1 seconds at 1,000 °C.

## CONCLUSIONS

1. Simulating the dry sorbent furnace injection process by using ambient temperature air as the injection medium increased the heating time of 37 to 105 μm diameter particles and delayed the calcination process.
2. The extent of calcination was insensitive to particle size in the range studied. The calcination model based on the specific BET surface area of the raw sorbent produced the best fit of the experimental data.
3. The calcination delay significantly affected the apparent sulfation rate for up to 0.2 seconds after sorbent injection. Between 0.2 and 1.0 seconds, the apparent sulfation rate was almost constant.
4. High purity limestones may not be the best choice for use in dry sorbent furnace injection processes. Low calcium dolostone may display better sulfation performance.

## ACKNOWLEDGMENTS

Financial support for this work was provided by Manufacturing and Technology Conversion International, Inc. under DOE Contract #DE.AC21-89MC26288. The cooperation of the staff of The Combustion Laboratory is also acknowledged.

## REFERENCES

1. Proceedings: *1990 $SO_2$ Control Symposium*, Session 3A, EPRI GS-6963, Electric Power Research Institute, Sept. 1990
2. Proceedings: *First Combined Flue Gas Desulfurization and Dry $SO_2$ Control Symposium*, Session 4A, EPRI GS-6307, Electric Power Research Institute, April 1989
3. Abichandani, J. S., *Gas Stream Cleanup Papers from DOE/METC Sponsored Contractors Review Meetings*, DOE/METC-89/6099, Morgantown, WV, 1988, p.167
4. Lawson, W. F., Maloney, D. J., Shaw, D. W. Richards, G. A., Anderson, R. J., Cook, J. M., Siriwardane, R. V., Poston, J. A. and Colaluca, M. A., *Proceedings of Seventh Annual Coal-fueled Heat Engines and Gas Stream Cleanup Systems Contractors Review Meeting*, DOE/METC-90/6110, Morgantown, WV, 1990, p.283
5. Borgwardt, R. H., *AIChE J.*, 1985, **31**, 103
6. Borgwardt, R. H. and Bruce, K. R, *AIChE J.*, 1986, **32**, 239
7. Borgwardt, R. H., Roache, N. F. and Bruce, K. R., *Ind. Eng. Chem. Fundam.*, 1986, **25**, 165
8. Powell, E. K. and Searcy, A. W., *Metallurgical Trans.*, 1980, **11B**, 427
9. Newton, G. H., Chen, S. L. and Kramlich, J. C., *AIChE J.*, 1989, **35**, 988

10.Milne, C. R., Silcox, G. D. and Pershing, D. W., *Ind. Eng. Chem. Res.*, 1990, **29**, 139
11.Milne, C. R., Silcox, G. D. and Pershing, D. W., *Ind. Eng. Chem. Res.*, 1990, **29**, 2201
12.Dam-Johansen, K., Hansen, P. F. B. and Østergaard, K., *Chem. Eng. Sci.* 1991, **46**, 847
13.Cole, J. A., Kramlich, J. C., Seeker, W. R., Silcox, G. D., Newton, D. W., Harrison, D. J. and Pershing, D. W., Proceedings: *1986 Joint Symposium on Dry $SO_2$ and Simultaneous $SO_2/NO_x$ Control Technologies*, Vol. 1, 16-1, EPRI CS-4966, Electric Power Research Institute, Dec. 1986

Table 1. Stratigraphic formations, chemical compositions and BET surface areas of the sorbents

| Formation | $CaCO_3$ | $MgCO_3$ | $SiO_2$ | $Al_2O_3$ | $Fe_2O_3$ | BET surface area ($m^2/g$) | | |
|---|---|---|---|---|---|---|---|---|
| | | | | | | 45μm | 63μm | 89μm |
| Linden Hall | 99.42 | 0.86 | 0.69 | 0.31 | 0.07 | 0.422 | 0.396 | 0.351 |
| Bossardsville | 86.93 | 1.91 | 8.07 | 1.46 | 0.95 | 0.648 | 0.613 | 0.579 |
| Nittany | 49.62 | 39.30 | 8.01 | 1.41 | 0.53 | 0.534 | 0.477 | 0.376 |

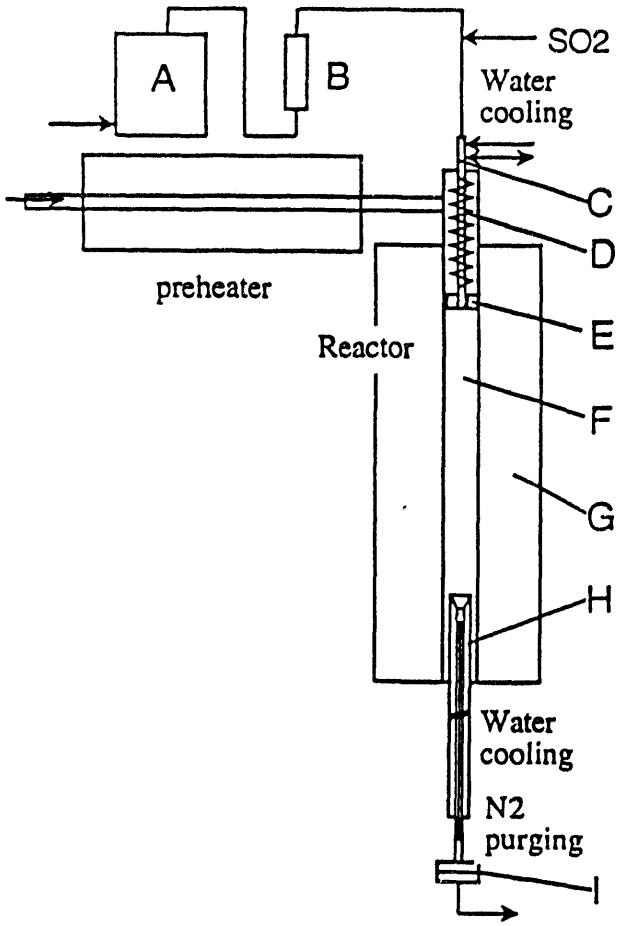


A fluidized-bed feeder, B flow stabilizer
C sorbent and SO2 injector
D injector outside heating
E flow straightener, F reactor tube
G electric furnace, H solid sampling probe
I sample filter

Fig. 1 Schematic diagram of entrained-flow reactor

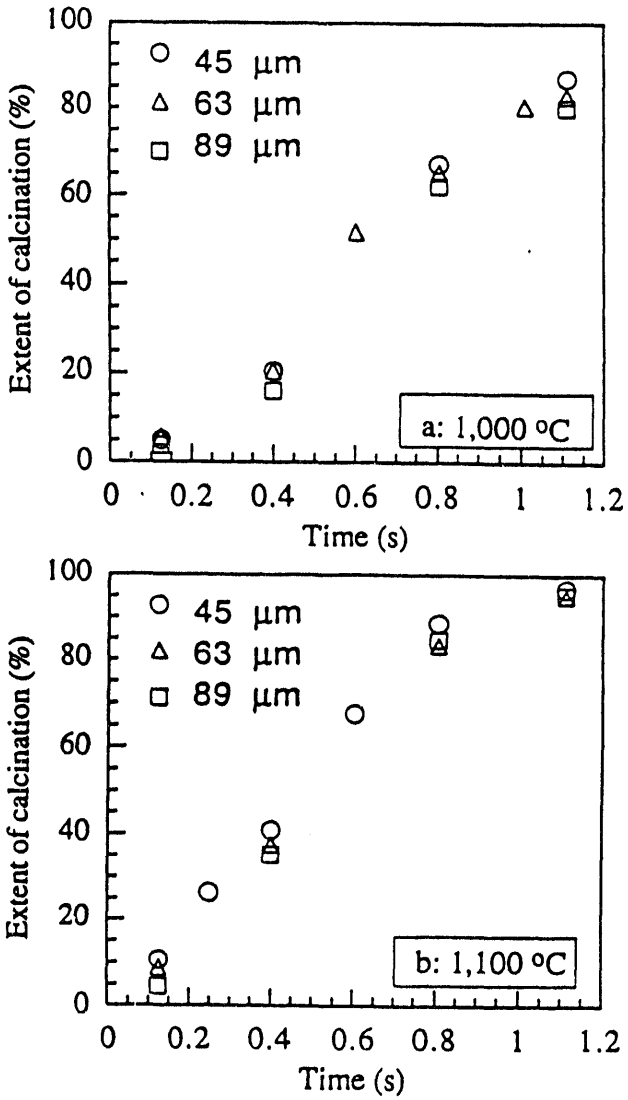


Fig. 2 Time dependency of the extent of calcination of the Linden Hall limestone at a) 1,000°C and b) 1,100°C for various particle sizes

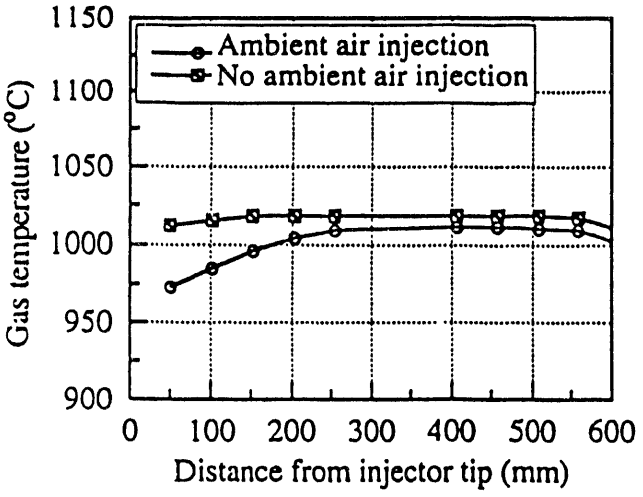


Fig. 3 Effect of injecting sorbent with ambient air on the gas temperature profile along the reactor

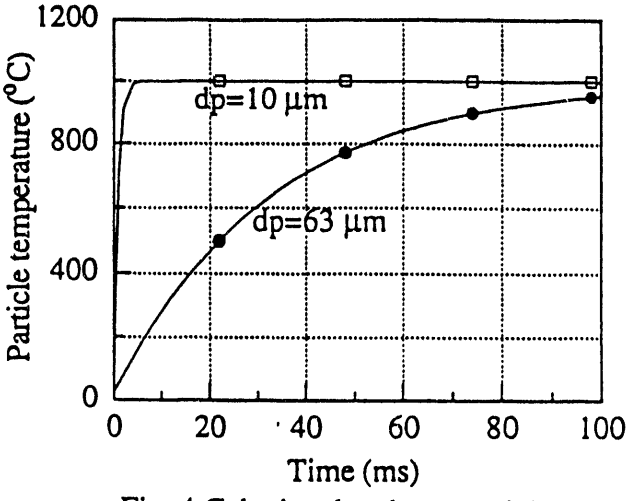


Fig. 4 Calculated sorbent particle temperature profiles during convective heating for 10 and 63 µm particles

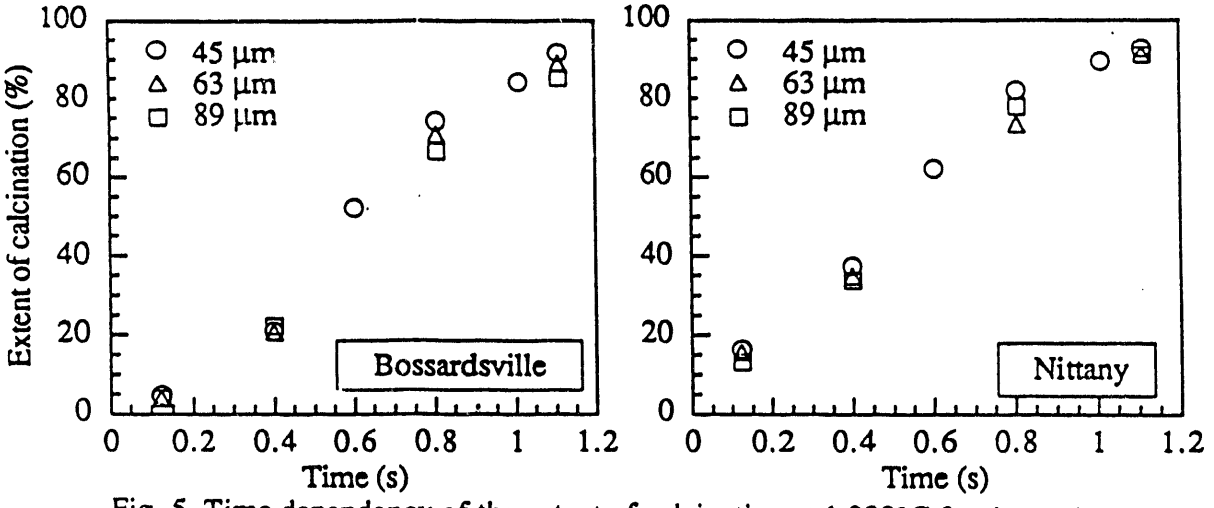


Fig. 5 Time dependency of the extent of calcination at 1,000°C for the various particle sizes of the Bossardsville and Nittany sorbents

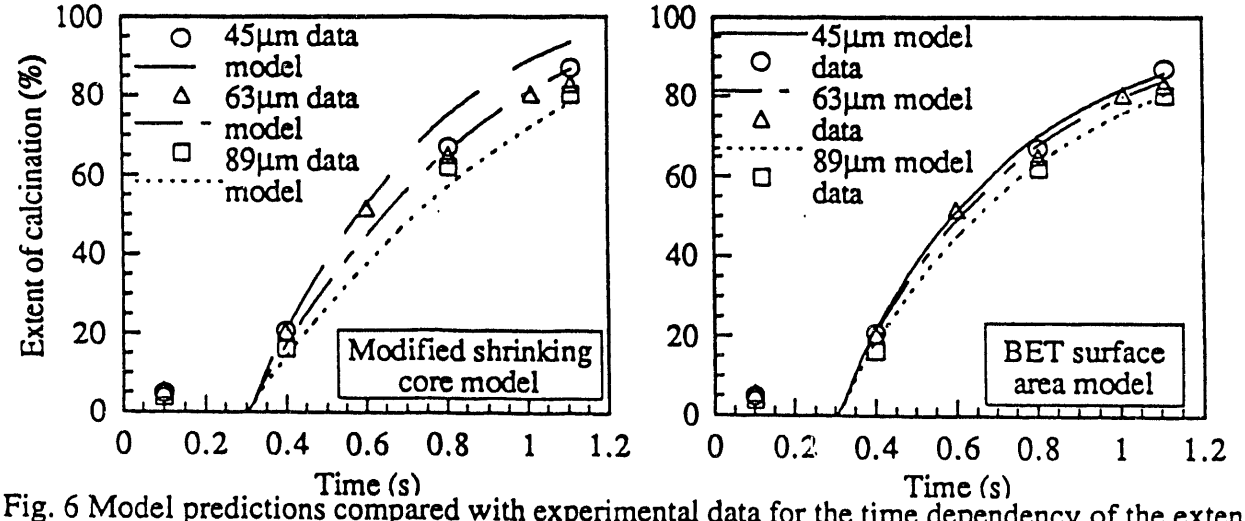


Fig. 6 Model predictions compared with experimental data for the time dependency of the extent of calcination at 1,000°C for various particle sizes of the Linden Hall limestone

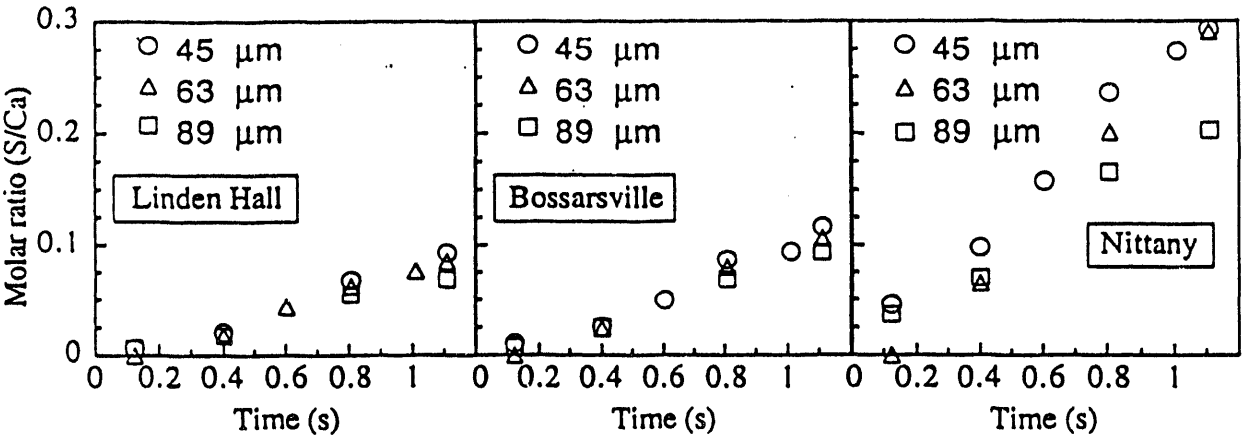


Fig. 7 Time dependency of the extent of sulfation at 1,000°C for the Linden Hall, Bossardsville and Nittany sorbents

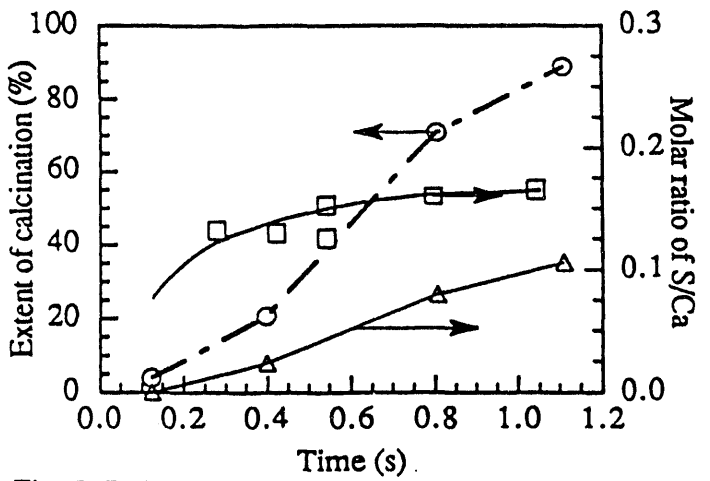


Fig. 8 Relationship between the time dependency of the extents of calcination and sulfation at 1,000°C of 63 μm Bossardsville limestone particles

DATE
FILMED
5/10/94
END